

# New perspectives on South Atlantic storm track through an automatic method for detecting extratropical cyclones' lifecycle

Danilo Couto de Souza<sup>1</sup>  | Pedro Leite da Silva Dias<sup>1</sup>  |  
Carolina Barnez Gramcianinov<sup>2</sup>  | Matheus Bonjour Laviola da Silva<sup>1,3</sup>  |  
Ricardo de Camargo<sup>1</sup> 

<sup>1</sup>Institute of Astronomy, Geophysics and Atmospheric Sciences, São Paulo University, São Paulo, Brazil

<sup>2</sup>Institute for Coastal Systems – Analysis and Modeling, Helmholtz-Zentrum Hereon, Geesthacht, Germany

<sup>3</sup>OceanPact, Rio de Janeiro, Brazil

## Correspondence

Danilo Couto de Souza, Institute of Astronomy, Geophysics and Atmospheric Sciences, São Paulo University, Rua do Matão, 226, Cidade Universitária, 05508-090 São Paulo, Brazil.  
Email: [dani.oceano@gmail.com](mailto:dani.oceano@gmail.com)

## Funding information

Coordenação de Aperfeiçoamento de Pessoal de Nível Superior-Brasil (CAPES), Grant/Award Number: Finance Code 001

## Abstract

This study introduces new insights into the climatology of South Atlantic (SAT) cyclones by employing a novel cyclone life cycle detection method, the CycloPhaser. Utilizing the minimum relative vorticity series and its derivative at the cyclone centre, the program effectively identifies distinct phases in the cyclone life cycle. Cyclone tracks are obtained through the analysis of relative vorticity at 850 hPa, using the ERA5 dataset. The study identified six main cyclone life cycle patterns from the analysis of 28,458 systems. The predominant cyclone type, accounting for approximately 60% of the analysed systems, exhibited a four-phase configuration: incipient, intensification, mature and decay. Detailed statistics for each developmental phase and the overall life cycle are presented, offering valuable comparisons and new insights while corroborating previous research findings. Key genesis regions in the SAT are identified, along with track density maps that reveal distinct preferences in cyclone developmental cycle. The main outcome of this study is the demonstration that the automated classification procedure enables the analysis of cyclones' life cycles to be conducted promptly and with low computing costs, facilitating the comprehensive study of cyclone behaviour with high efficiency.

## KEY WORDS

automatic method, cyclone's lifetime, open source, South Atlantic

## 1 | INTRODUCTION

Cyclones play a crucial role in regulating global weather and climate. In the South Atlantic (SAT), surface cyclones significantly influence the precipitation regimes in South America (Reboita et al., 2010b, 2018) and are associated with extreme precipitation events (de Souza & da Silva, 2021). Additionally, they pose natural hazards along the South American coast through intense winds

(Cardoso et al., 2022; de Souza & da Silva, 2021), high sea waves (Gramcianinov et al., 2023; Guimarães et al., 2014) and storm surges (Campos et al., 2010; Leal et al., 2023), triggering episodes of coastal erosion (Parise et al., 2009), resulting in economic losses in sectors such as oil exploration, fishing and coastal infrastructure, and impacting navigation. Therefore, enhancing our understanding of these systems, including their climatological aspects and the dynamical mechanisms leading to their formation

and evolution, is essential for improving forecasts and implementing effective mitigation and adaptation strategies.

The SAT features various regions conducive to cyclogenesis. Along the southeastern coast of South America, three genesis regions are identified: one in southeastern Argentina (ARG), another near the La Plata river discharge in Uruguay (LA-PLATA) and a third near Southeast Brazil (SE-BR) (Crespo et al., 2021; Gan & Rao, 1991; Gramcianinov et al., 2019; Hoskins & Hodges, 2005; Reboita et al., 2010a; Sinclair, 1995). Other genesis regions are located in the southeastern sector of the SAT (SE-SAO), the Weddell Sea (WEDDELL), the Antarctic Peninsula (AT-PEN) and west of the South African and Namibian coast (SA-NAM) (Carrasco et al., 2003; Gramcianinov et al., 2019; Heinemann, 1990; Hodges et al., 2011; Hoskins & Hodges, 2005; Simmonds & Keay, 2000).

Cyclogenesis along the South American coast primarily arises from baroclinic instability and lee cyclogenesis (Gan & Rao, 1994; Gramcianinov et al., 2019; Vera et al., 2002). In the ARG region, cyclogenesis is modulated by the position of the upper-level jet, similar to winter genesis in LA-PLATA and SE-BR (Crespo et al., 2021; Gramcianinov et al., 2019). During summer, LA-PLATA benefits from warm advection driven by thermal-orographic lows, while SE-BR cyclones form under barotropic conditions, enhanced by moisture advection from the Subtropical High (Crespo et al., 2021; Gozzo et al., 2017; Gramcianinov et al., 2019). Additionally, oceanic influences such as the warm Brazil Current and the pronounced sea-surface temperature gradients of the Brazil-Malvinas Confluence critically support coastal cyclogenesis by providing essential moisture, heat and low-level baroclinicity (Gramcianinov et al., 2019; Sanders & Gyakum, 1980; Vera et al., 2002).

Few studies have examined the genesis mechanisms for the SE-SAO, AT-PEN, WEDDELL and SA-NAM regions. Gramcianinov et al. (2019) suggest that winter cyclogenesis in SE-SAO is highly baroclinic, often related to secondary cyclogenesis in the cold sector of a pre-existing cyclone. Along the SA-NAM coast, cyclogenesis is likely influenced by the South African Plateau (Inatsu & Hoskins, 2004), potentially mirroring genesis mechanisms of coastal lows west of the Andes (e.g., Crespo et al., 2023). Less explored regions like AT-PEN and WEDDELL may involve polar lows or meso-scale cyclones that can evolve into more intense synoptic disturbances (Carrasco et al., 2003; Heinemann, 1990; Turner & Thomas, 1994). In these areas, lee cyclogenesis might occur due to complex topographical influences, with systems in WEDDELL often developing from cold air pools over ice-free sea areas, influenced by offshore

winds (Heinemann, 1990; Turner & Thomas, 1994). Additionally, the interaction between sea ice and cyclogenesis at WEDDELL is significant. Recent studies highlight the impact of sea ice on surface albedo, thermal conductivity and atmospheric heat exchange processes (Vihma, 2014). A correlation between decreased sea ice and an enhanced number of cyclones has been observed, although these tend to be weaker (Simmonds & Wu, 1993), while intense systems have the capacity to reduce local sea-ice extent (Jena et al., 2022).

While climatologies of cyclones in the SAT, including genesis regions, are comprehensive, understanding the specific regions where cyclones intensify, mature and decay remains limited—a challenge not unique to the SAT but prevalent globally. The pioneering work by Bjerknes (1922) first described extratropical cyclone life cycles, identifying distinct phases using structural changes and large-scale dynamics, a methodology further refined by Shapiro and Keyser (1990) and Neiman and Shapiro (1993), who delineated phases like the incipient broad baroclinic, frontal fracture, T-bone and warm-core seclusion. Recent research has aimed to objectively define these stages. Bengtsson et al. (2009) analysed Northern Hemisphere extratropical cyclones, while not specifying development stages, noted discernible phases around maximum system intensity. Schemm et al. (2018) normalized cyclone life cycles to identify front-associated periods, and Rudeva and Gulev (2007) introduced a “non-dimensional cyclone lifetime” to examine changes in cyclone radius throughout its life cycle. Other studies have identified the mature phase using peak vorticity or the lowest central pressure and segmented the life cycle into intensification and decay stages relative to peak intensity (Azad & Sorteberg, 2014; Booth et al., 2018; Dacre & Gray, 2009; Michaelis et al., 2017; Trigo, 2006). For analysing intensification, Grise et al. (2013) used a growth rate value, whereas Pinto et al. (2005) employed the baroclinic Eady growth rate.

Despite these advancements, existing methods primarily focus on analysing the intensification and decaying stages and do not provide comprehensive tools for determining and analysing the mature and incipient stages—periods when surface isobars are not yet fully closed, but environmental dynamics are already changing due to the presence of a low-level disturbance. Moreover, there is a lack of robust methodologies suitable for climatological studies that enable detailed analysis and classification of distinct stages in cyclones' life cycles. This study proposes an objective method for determining the stages of development of cyclones using their central vorticity. The method is applied to study features of the life cycle of cyclones in the SAT region, providing new insights into cyclone behaviour, such as displacement length, speed

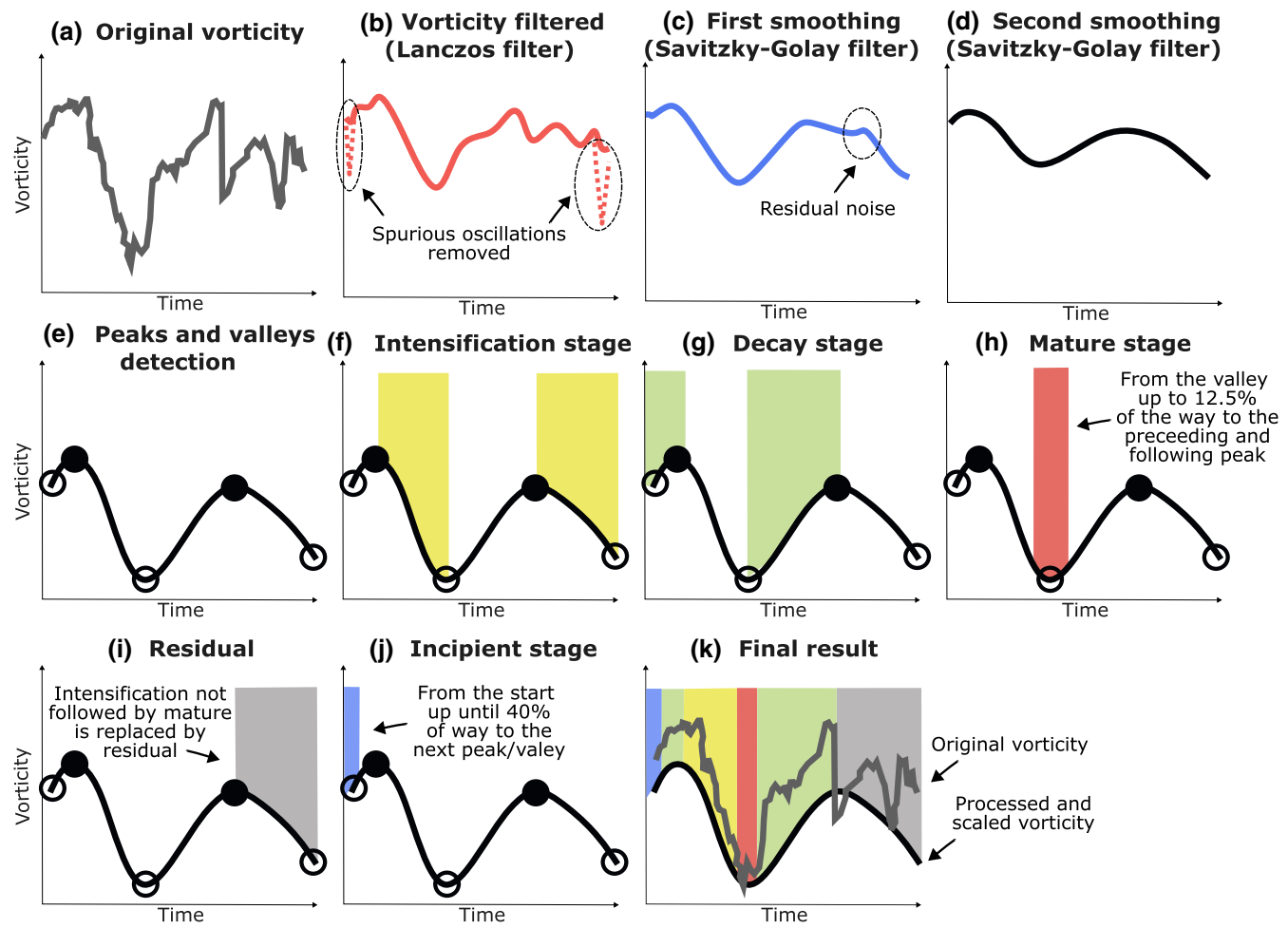


**FIGURE 1** Sequential methodology of the CycloPhaser program for cyclone life cycle analysis. (a) Original vorticity series input. (b) Noise reduction using the Lanczos filter, supplemented by a low-pass filter on the initial and final 5% to remove spurious oscillations. (c, d) Series smoothing through first and second applications of the Savitzky–Golay filter. (e) Peaks and valleys identification in the prepared series. (f–j) Detection and labelling of the cyclone development stages: intensification, decay, mature, residual and incipient, respectively. (k) Comprehensive overview combining all detected stages with the original and processed vorticity series. [Colour figure can be viewed at [wileyonlinelibrary.com](http://wileyonlinelibrary.com)]

and duration, as well as the preferred regions of occurrence for each phase. The main outcome of this study is that the automated classification procedure enables large quantities of data to be processed promptly, opening doors for future studies, such as analysing cyclone life cycle behaviour in climate projections, including those from CMIP6 models, and comparing them to the present-day climatology.

## 2 | METHODS

### 2.1 | The CycloPhaser program

We developed CycloPhaser, an automated Python package for detecting cyclone life cycle phases. This open-source Python package is freely available in the PyPI

repository (<https://pypi.org/project/cyclophaser>) and can be installed via the pip package manager. Comprehensive documentation for the package, along with illustrative examples of its usage, is accessible on the PyPI project website. It identifies the phases by analysing the relative vorticity at the cyclone centre and its first derivative (Figure 1). Primarily designed for central relative vorticity analysis, as utilized in our study, CycloPhaser also accommodates sea-level pressure or geopotential height data.

The program starts with a pre-processing stage. On it, the users have the option to apply the Lanczos filter (Duchon, 1979) to the vorticity time series to remove noise in the data (Figure 1b), mostly unrelated to the development of extratropical cyclones on synoptic scales, including fluctuations in wind components induced by features like topography-induced circulations, sea breezes

and spatial and temporal variations in sea surface structures (e.g., Acevedo et al., 2010; Da et al., 2017; Steele et al., 2015). High-resolution datasets, such as ERA5, benefit from this filtering due to their sensitivity to noise from structures like frontal systems (Hoskins & Hodges, 2002). However, this step can be skipped for datasets already processed by tracking algorithms that include spatial filtering (Flaounas et al., 2014; Hoskins & Hodges, 2002; Murray & Simmonds, 1991; Pinto et al., 2005). The Lanczos filter, functioning as a band-pass, permits customization of cutoff frequencies for precise filtering. To counteract potential spurious oscillations at data series endpoints introduced by spectral filtering, a weaker low-pass Lanczos filter can be applied to the initial and final 5% of the data series, ensuring smoother endpoints (Figure 1b).

After filtering, the CycloPhaser program uses a Savitzky–Golay filter (Savitzky & Golay, 1964) to further reduce residual noise, crucial for ensuring the derivative curves form a sinusoidal pattern for precise phase detection (Figure 1c). Users can apply this smoothing twice (Figure 1d), adjusting its intensity to balance noise reduction and data integrity, tailoring the process to specific requirements. Following this, the first derivative of relative vorticity is calculated primarily using second-order finite differences, employing central differences for interior points and forward/backward (first-order) differences for the endpoints. This derivative is then subjected to double smoothing with the Savitzky–Golay filter to maintain a sinusoidal pattern in the derivative series, a critical step for accurately identifying cyclone life cycle phases. Skipping this dual smoothing could lead to false phase detections, emphasizing its necessity for reliable analysis.

The first phases to be detected are the intensification and decay stages. In those stages, the program employs a method based on detecting peaks and valleys in the relative vorticity time series (Figure 1e). The intensification phase is defined by the intervals from one peak to the subsequent valley (Figure 1f), while the decay stage is determined by the spans from one valley to the following peak (Figure 1g). Each intensification/decay interval must span at least 7.5% of the total series length to be considered significant. To ensure accuracy, the program checks for multiple blocks of consecutive intensification/decay periods and merges them if the gap between them is smaller than 7.5% of the series length.

The program then proceeds to detect the mature stage of the cyclone's life cycle (Figure 1h). Similar to the previous step, it identifies peaks and valleys in the relative vorticity, however in this case, it also considers the derivative of vorticity (already smoothed). Between a peak (valley) and a valley (peak) of vorticity series, there is always a valley (peak) of its derivative, which

corresponds to the periods of maximum intensification (decay) of vorticity. Therefore, the mature stage was defined as the intervals between the valley of vorticity and 12.5% of the time between the preceding derivative valley, as well as 12.5% of the time to the following derivative peak. To be recognized as a significant mature stage, each interval must span at least 3% of the total series length. Additionally, the program verifies that all mature stages are preceded by an intensification stage and followed by a decay stage, ensuring the accurate identification of the mature phase within the cyclone's life cycle.

The specific thresholds for phase detection, including the 7.5% span for intensification/decay intervals and the 3% minimum for the mature stage, along with the 12.5% intervals defining the bounds of the mature stage, were established through rigorous testing. This testing involved an iterative calibration process, where various percentage thresholds were applied to a representative sample of cyclone tracks to determine the most accurate parameters for phase delineation. The final percentages were selected based on their effectiveness in capturing the genuine progression of cyclogenesis while filtering out inconsequential fluctuations in vorticity. This careful calibration ensures that the CycloPhaser program reliably identifies each phase, providing a consistent and objective methodology for analysing the life cycle of extratropical cyclones. For a understanding of how variations in these thresholds affect phase detection, please refer to Figures S1–S4, Supporting Information which offer a comparative analysis using a set of cyclone case studies.

Next, our methodology introduces the “residual” stage to address peculiarities of tracking algorithms rather than signifying a distinct phase in extratropical cyclone evolution (Figure 1i). The CycloPhaser program tags stages as “residual” by analysing detected cyclone phases; if a mature stage does not transition to a decay stage or if an intensification stage post a full cycle (intensification, mature, decay) does not lead to another mature phase, these instances are classified as “residual” (Figure 1e). This criterion accounts for scenarios where the tracking algorithm may continue to follow a cyclone post-decay, potentially capturing a re-intensification that does not culminate in a mature stage due to tracking limitations. For instance, Figure 1e depicts a system re-intensifying post-decay without progressing to a mature phase, interpreted as a tracking anomaly.

Following, a post-processing is applied, where the program refines cyclone phase identification by bridging gaps between successive intensification and decay phases. It checks for discontinuities within consecutive phase blocks, filling any found with the adjacent phase to ensure continuous phase transitions. Moreover, it

corrects isolated phases lasting only one time step by aligning them with either the subsequent phase (at series start) or the preceding phase (elsewhere), enhancing phase consistency throughout the cyclone lifecycle.

In the cyclone phase identification's final step, the program discerns the “incipient” stage (Figure 1j) by first labelling any unassigned phases as “incipient.” It then analyses the phase sequence for an incipient-to-intensification or incipient-to-decay transition. For incipient-to-intensification, “incipient” labels cover the initial 40% towards the next vorticity derivative valley. For incipient-to-decay, they extend 40% towards the next peak (Figure 1f). This 40% threshold, established through testing, ensures the precise delineation of cyclone phases, accommodating cyclones that initiate with ambiguous or rapid phase transitions.

## 2.2 | Southern Atlantic cyclone detection and life cycle determination

The cyclone track information used in the current study was obtained from the “Atlantic extratropical cyclone tracks database” available at Gramcianinov et al. (2020b), which covers the entire Atlantic Ocean from 1979 to 2020. The spatial domain chosen for the analysis lies between 15°S–55°S and 75°W–20°E. Cyclones are tracked based on ERA5 fields (winds at 850 hPa) using the TRACK algorithm (Hodges, 1994, 1995) and Hoskins and Hodges (2002) method, following the minimum duration and displacement requirements of 24 h and 1000 km, respectively. ERA5 was selected for its finer resolution compared to alternatives like CFSR/CFSv2, offering significant advantages in analysing regions characterized by complex orography and temperature gradients, thereby ensuring a comprehensive and consistent representation of cyclones (Gramcianinov et al., 2020a). This approach aligns with the characteristics and counts observed in previous South Atlantic cyclogenesis studies. Systems spending over 80% of their life cycle over the continent were excluded to omit thermal lows and lee troughs (e.g., Crespo et al., 2021), employing mobility criteria consistent with earlier South Atlantic cyclone climatologies (e.g., Gramcianinov et al., 2019; Sinclair, 1995). Further details on the methodology and database evaluation are discussed in Gramcianinov et al. (2020a).

The primary focus on extratropical cyclones in this study stems from the specific calibration and design of the TRACK algorithm used for cyclone tracking. While the methodology does not explicitly exclude subtropical or tropical cyclones, the detection of such systems is less likely due to their rarity in the South Atlantic and the algorithm's sensitivity to the features typical of

extratropical cyclones. It is important to note that subtropical systems, which share characteristics with both tropical and extratropical cyclones (e.g., Hart, 2003), may occasionally be detected, but they constitute a minority within the dataset. In the historical record for the region, there have only been two notable cases of tropical cyclones: Hurricane Catarina (Pezza & Simmonds, 2005) and Tropical Storm Iba (Reboita et al., 2021).

In this study, the CycloPhaser's default settings were primarily used to identify cyclone life cycle phases. The TRACK program's spatial filtering (Hodges, 1994, 1995) negated the need for applying the Lanczos filter on relative vorticity series. The Savitzky–Golay filter's window length was tailored to each system's life cycle duration; for those exceeding 8 days, it was set to an odd integer near 25% of the series length, while for shorter life cycles, it was adjusted to an odd integer near 50% of the series length. During the second smoothing, for life cycles over 8 days, the window length was an odd integer close to 50% of the series length, but for shorter cycles, it was kept consistent with the first smoothing step.

## 3 | RESULTS AND DISCUSSION

### 3.1 | Life cycle types

The TRACK algorithm identified 33,376 cyclone systems from 1979 to 2020, using criteria described in section 2.2. Initially, 39 cyclone life cycle types were detected, but to focus our analysis, we concentrated on configurations comprising at least 1% of all types, as shown in Figure 2a. This refinement led to a focus on types representing 95% of systems (31,719), justifying the removal of the less significant types. Notably, several identified types included a “residual” stage, not indicative of an actual development phase. To adjust, we merged counts of life cycle types differing only by this stage. Also, systems without a mature stage were excluded to prevent skewing phase statistics, recognizing that such systems might have unique processes or could be undeveloped troughs, requiring further investigation. This refined approach led to analysing 28,458 systems, about 85% of total SAt-origin systems, ensuring a more accurate representation of cyclone life cycles (Figure 2b).

The life cycle of representative systems of the six life cycle types presenting more than 1% of occurrence in the SAt and that presents at least one mature stage is displayed at Figure 3. By far, the most common cyclone type follow a four-phase configuration: incipient, intensification, mature and decay, collectively accounting for approximately 60% of the analysed systems (Figure 3a). This configuration represents a complete extratropical cyclone development cycle. The second most prevalent

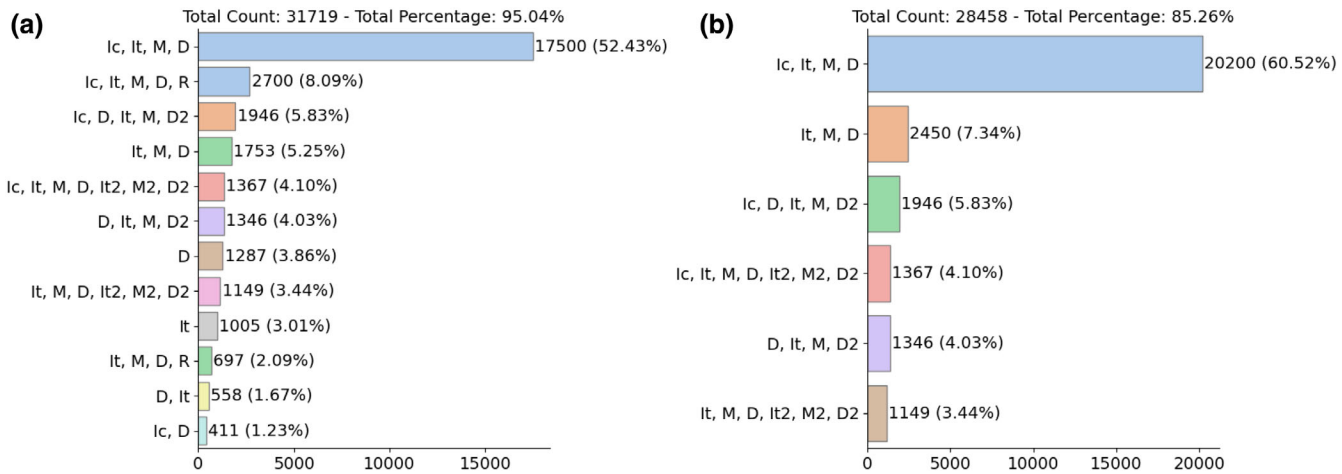


**FIGURE 2** Distribution of identified cyclone life cycle types as a percentage of the total number of cases studied (33,376), with each type representing at least 1% of the total cases. (a) Initial count distribution of life cycle types, including those with a “residual” phase; bars of the same colour indicate structurally similar life cycle configurations that differ only by the presence or absence of the residual phase. (b) Distribution after aggregating similar life cycle types by removing the “residual” phase and excluding configurations without a “mature” phase. The phases are labelled: “incipient” (Ic), “intensification” (It), “mature” (M), “decay” (D), “residual” (R), with a second occurrence denoted by (2). [Colour figure can be viewed at [wileyonlinelibrary.com](#)]

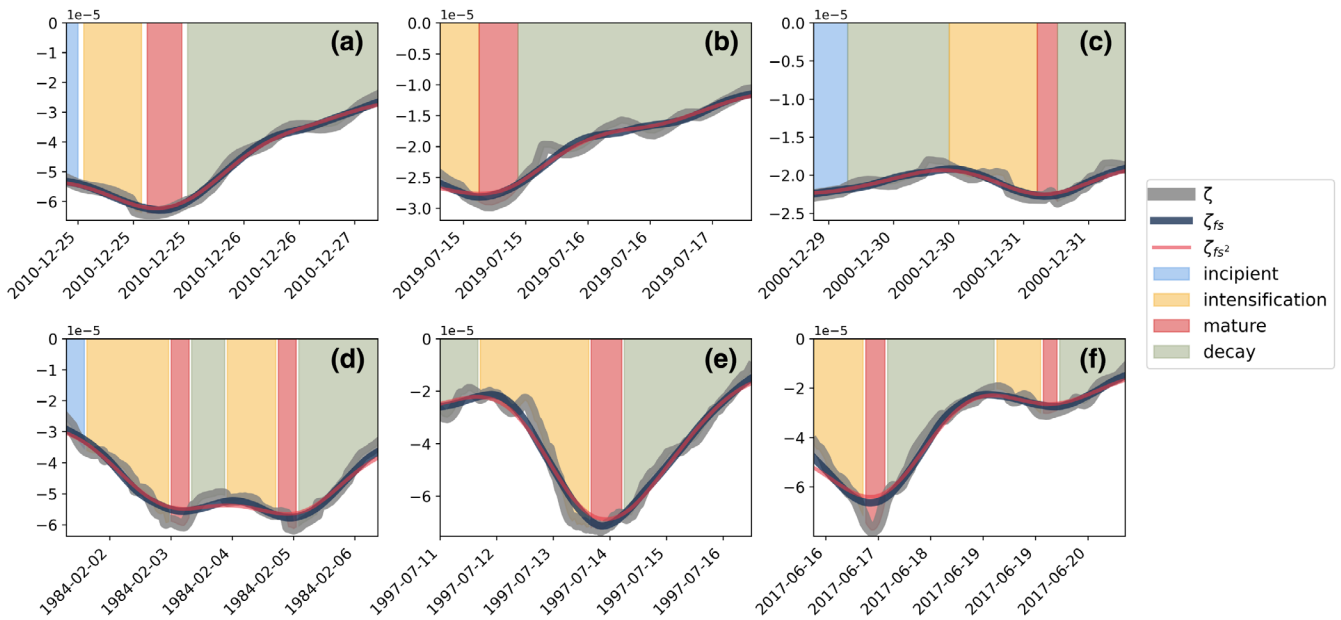
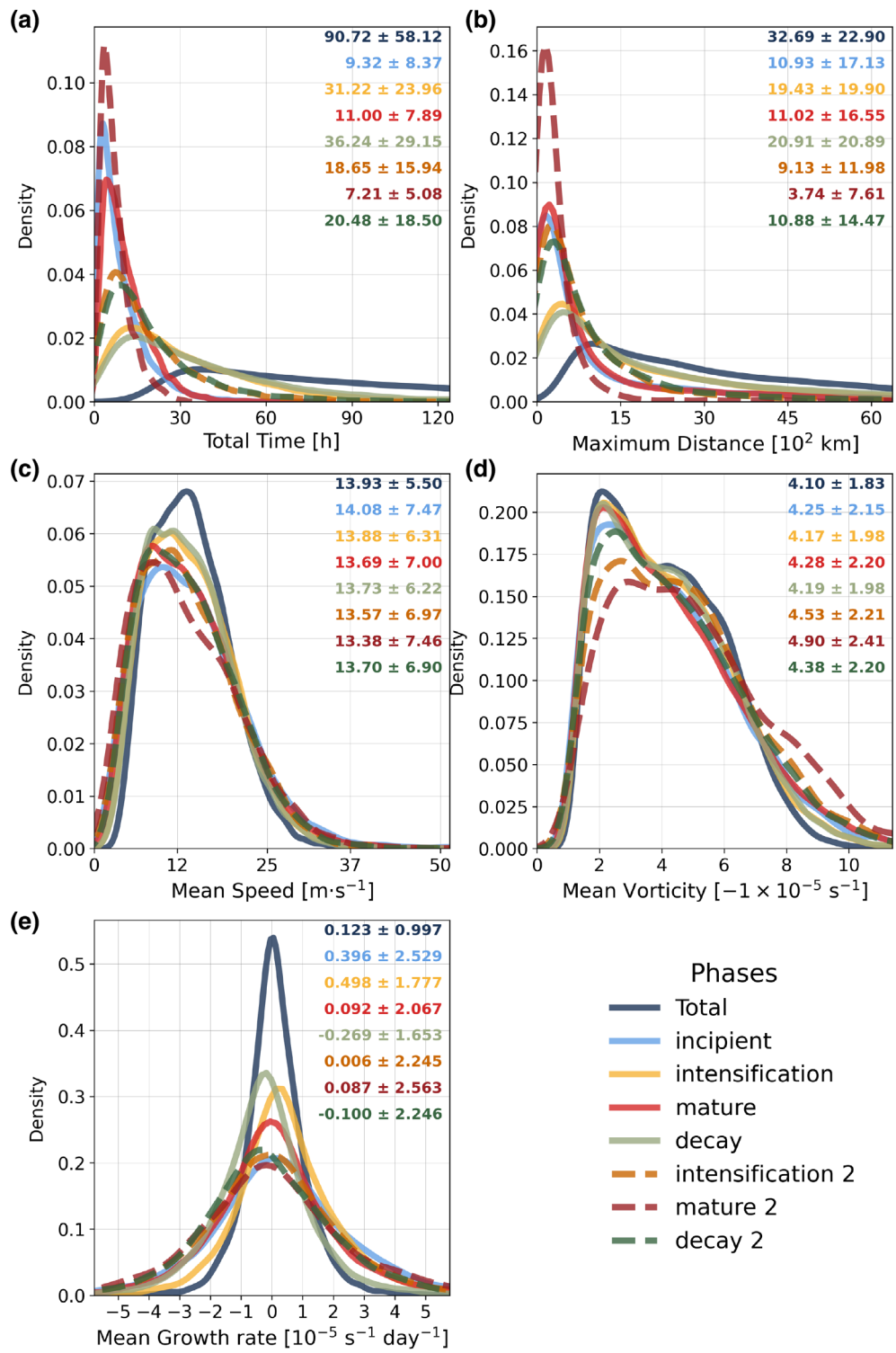


**FIGURE 3** Illustrative examples of cyclone life cycles corresponding to the categories defined in Figure 2b. Each panel (a-f) displays the temporal evolution of vorticity and its smoothed derivatives, with coloured backgrounds indicating the different stages of a cyclone's life cycle. The lines represent the original vorticity series ( $\zeta$ ) and the first ( $\zeta_{fs}$ ) and second ( $\zeta_{fs}^2$ ) smoothed relative vorticity. [Colour figure can be viewed at [wileyonlinelibrary.com](#)]

type, representing 7.3% of occurrences, follows the full developmental cycle but lacks the incipient stage (Figure 3b). The third and fifth most frequent types, accounting for 5.8% and 4.0%, respectively, feature an early decay. The former includes an incipient stage (Figure 3c), while the latter does not (Figure 3e). Lastly, the fourth and sixth configurations entail the complete

cyclone development cycle twice, presenting a secondary intensification, mature and decay phases. The former presents an incipient stage (Figure 3d) and the latter, does not (Figure 3f). Remarkably, the frequency of these types exhibits minimal to no seasonal (Figure S5) or spatial (Figure S6) variability for their respective genesis regions (as defined in section 3.3.1).

**FIGURE 4** Statistics for the total system's life cycle and each individual phase: (a) total duration (h), (b) maximum travelled distance (km), (c) mean speed (in  $\text{m}\cdot\text{s}^{-1}$ ), (d) mean vorticity (scaled by  $-1 \times 10^{-5} \text{s}^{-1}$ ), (e) mean growth rate ( $10^{-5} \text{s}^{-1} \cdot \text{day}^{-1}$ ). [Colour figure can be viewed at [wileyonlinelibrary.com](http://wileyonlinelibrary.com)]



### 3.2 | Cyclone life cycle statistics

The average lifetime of SAT cyclones with at least one mature stage is  $90.72 \pm 58.12$  h ( $3.78 \pm 2.42$  days), peaking in duration between 30 and 60 h (1.25 and 2.5 days), and an average displacement of  $3269 \pm 2290$  km, mostly ranging from 1000 to 1500 km (Figure 4a,b). These findings are generally in line with those by Gramcianinov

et al. (2019, 2020a), but slightly higher than Simmonds and Keay (2000), Mendes et al. (2010) and Reboita et al. (2010a). Furthermore, Mendes et al. (2010) documented longer lifetimes but shorter displacements than our results. The observed differences are likely attributed to varying tracking methodologies, datasets and our exclusion of systems without a mature phase. Especially, the exclusion of continental systems might have contributed

to higher displacements, as on austral summer and autumn, there are quasi-stationary lows over the South American continent (Mendes et al., 2010). Additionally, Reboita et al.'s (2010a) study focus on oceanic-only systems overshadows the initial development stages of some systems, as shown by Gramcianinov et al. (2019).

In detail, the PDFs for both duration and displacement are left-skewed (Figure 4a,b), indicating that longer or farther-reaching phases are less common. The shortest average durations and displacements are seen in the incipient, mature and second mature phases, which present the highest frequencies at approximately 3 h and 3000 km, highlighting that these stages of development in SAT cyclones may often go undetected in standard 6-hourly analyses. Conversely, the first intensification and decay phases show the longest durations and greatest displacements, with notably shorter subsequent occurrences. Given that the third most frequent cyclone life cycle type undergoes early decay (Figure 2), it is important to bear in mind that the mean values observed for the first decay phase encompass both early decay stages as well as decay stages occurring after a mature phase.

The mean translational speed of approximately  $13.9 \pm 5.5 \text{ m}\cdot\text{s}^{-1}$  is on agreement with previous studies (e.g., Gramcianinov et al., 2019, 2020a; Hoskins & Hodges, 2005) but higher than mean values found by Reboita et al. (2010a). However, in that study, the authors used relative vorticity at 10 m for the tracking procedure, which is affected by the surface drag. Surprisingly, the mean speed is similar among all phases, with the highest difference in  $0.4 \text{ m}\cdot\text{s}^{-1}$  but decreasing mean values from the incipient to mature stage. This pattern still holds for the second life cycle. Therefore, the cyclones in the SAT are slower at their mature phases, which are related to extreme wave occurrence (Gramcianinov et al., 2023).

The PDF for the lifecycle of examined systems shows a bimodal, left-skewed distribution with peaks near 2 and between 4 and  $5-1\times 10^{-5} \text{ s}^{-1}$ , with an average value of  $4.1\pm 1.8-1\times 10^{-5} \text{ s}^{-1}$  (Figure 4d). However, unlike traditional studies focusing on vorticity at specific points, the CycloPhaser approach offers a detailed analysis throughout various developmental stages of cyclonic systems, providing a deeper insight into the cyclone life cycle. Our results for the incipient stage exhibit higher vorticities compared to the initial vorticities reported by Gramcianinov et al. (2019), Gramcianinov et al. (2020a) and Reboita et al. (2010a). This discrepancy may be attributed to our exclusion criteria and the observed tendency for vorticity to decrease when an incipient stage is followed by an intensification phase (e.g., Figure 3a,d), possibly resulting in a bias towards lower values for this phase. Furthermore, in their analysis focusing on the first time step, the time step of minimum vorticity and the last time step,

Sinclair (1995) reported higher vorticity values compared to our findings for the incipient, mature and decay stages. However, these authors omitted the influence of topography by using geostrophic relative vorticity, which justifies the difference in vorticity distribution.

The analysis revealed that the systems are most intense during the mature phase, as expected, exhibiting a broad range of vorticity values, highlighting the variability in mature cyclones' peak intensities. The intensification and decay phases, by contrast, display more similar mean vorticities, reflecting their lifecycle roles: intensification lowers system vorticity from the base state, whereas decay phase brings it closer to the base state again. Secondary intensification and maturation phases typically show lower mean vorticities than their primary counterparts, occurring when a cyclone re-intensifies without returning to its original genesis vorticity. Thus, these phases experience similar intensification and decay levels but do not achieve the higher vorticities of initial phases, illustrating the nuanced relationship between cyclogenesis dynamics and the environmental conditions influencing the cyclone lifecycle.

The mean growth rate distribution is symmetric around zero (Figure 4e) and has low standard deviation, indicating a dynamic equilibrium in system intensity over the life cycle, with neither consistent intensification nor weakening. Despite this symmetry, individual stages show significant variability due to inherent noise in vorticity data, even after spatial filtering by the TRACK algorithm. The second mature stage distribution is slightly left skewed, potentially influenced by the Lanczos filter, suggests some instances of second intensification might be classified as part of the second mature phase (Figure 3c). Despite these nuances, the CycloPhaser adeptly outlines Southern Atlantic transient systems' lifecycles, marking the highest mean growth rates in intensification stages and the lowest in decay stages.

Unexpectedly, the incipient stage displays relatively high positive mean growth rate values. This finding aligns with the mean growth rate for cyclogenesis regions as reported by Hoskins and Hodges (2005) and Gramcianinov et al. (2019). Although the mean values for the second intensification and decay stages are lower than those of the initial stages, they show higher standard deviations, correlating with their mean intensity. This variation could stem from the smaller sample size of these stages and the increased variability in the secondary life cycle of systems undergoing this development.

### 3.3 | Track density maps

In this section, we present a detailed analysis of the spatial distribution of cyclone density across different

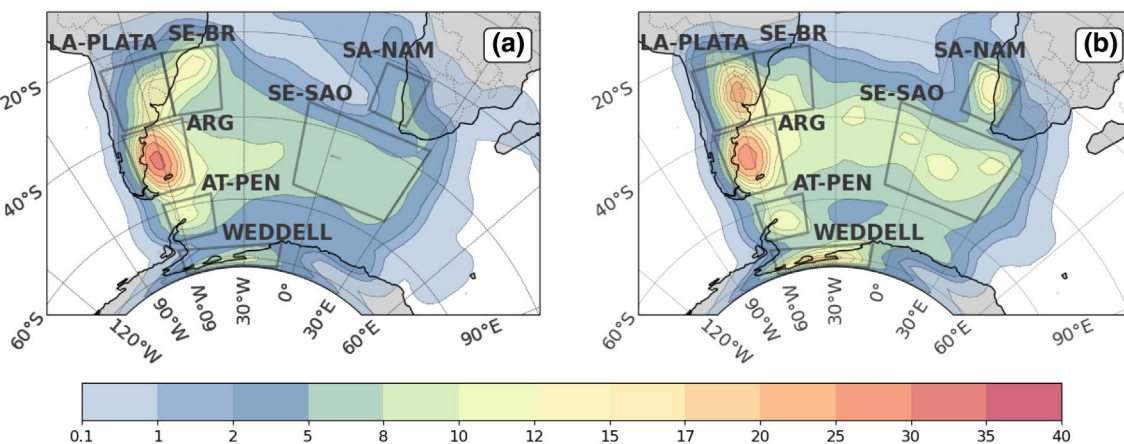


**FIGURE 5** Cyclone track density for incipient phase, for all systems with genesis in the South Atlantic, for (a) austral summer (DJF) and (b) austral winter (JJA), and each respective genesis region. The track density unit is cyclone per  $10^6 \text{ km}^2$  per month. [Colour figure can be viewed at [wileyonlinelibrary.com](http://wileyonlinelibrary.com)]

developmental phases, highlighting the key storm track regions in the Southern Atlantic. This analysis enhances our understanding of the extratropical cyclone development cycle within the study area, revealing patterns and trends that may have implications for regional weather and climate forecasting. The cyclone density is computed using the kernel density estimation (KDE) method (Hodges, 1996). We calculate the track density for each phase using the central point of the cyclones during all time steps in which the system is identified in a given phase. Note that this method differs from the traditional track density obtained by the TRACK program (e.g., Gramcianinov et al., 2020a; Hoskins & Hodges, 2002), which considers a specific or unique time step along the track to compute the track density. The raw density statistics are then scaled to represent the number of cyclones per month per unit area, allowing for a normalized comparison across different regions and phases. This scaling is crucial for accurately assessing the relative frequency and intensity of cyclone activity in different parts of the Southern Atlantic. The area unit used for this analysis is equivalent to a  $5^\circ$  spherical cap, which approximates to  $10^6 \text{ km}^2$ . This unit size was chosen to provide a balance between spatial resolution and statistical robustness, ensuring that the density maps effectively capture regional variations in cyclone activity while maintaining sufficient data points for reliable analysis.

### 3.3.1 | Incipient phase

During the incipient stage, it was observed the three cyclogenesis regions along the South American coast: SE-BR, LA-PLATA and ARG (Figure 5). Nevertheless, this analysis reveals the existence of several other cyclogenesis

regions that, while identified in previous studies, have not been as extensively discussed and understood as ARG, LA-PLATA and SE-BR. These regions are situated along the Southeast Atlantic (SE-SAO), South African and Namibian coast (SA-NAM), Antarctic Peninsula (AT-PEN) and Weddell Sea (WEDDELL). Figure 5 illustrates cyclone track density (cyclones per  $10^6 \text{ km}^2$  per month) for the austral summer (DJF) and winter (JJA) in the SAt. As transitional seasons demonstrate characteristics that lie between these two extremes, consistent with findings from earlier research (e.g., Crespo et al., 2021; Gan & Rao, 1991; Reboita et al., 2010a), our analysis will predominantly concentrate on DJF and JJA, along with the previously mentioned cyclogenesis regions.

The ARG region consistently maintains similar track densities throughout both DJF (Figure 5a) and JJA (Figure 5a), exceeding 30 cyclones per  $10^6 \text{ km}^2$  per month, respectively. In contrast, the LA-PLATA and SE-BR regions display a noticeable seasonality pattern. The LA-PLATA region experiences increased activity during JJA compared to DJF, with densities surpassing 20 and 10 cyclones per  $10^6 \text{ km}^2$  per month, respectively. Meanwhile, the SE-BR region presents heightened activity during DJF compared to JJA, with densities exceeding 10 cyclones per  $10^6 \text{ km}^2$  per month during DJF, whereas it exhibits negligible activity during JJA. It is important to note that the variations in track density, in comparison to the genesis densities reported by Gramcianinov et al. (2020a, 2019), stem from their focus solely on the initial time step of the system life cycle for analysis, whereas this study considers all periods classified as the incipient stage. Also, on Gramcianinov et al. (2019), the tracks steamed from the NCEP-CFSR reanalysis, whereas here, those were identified using the ERA5. For the genesis regions on the South American coast, the

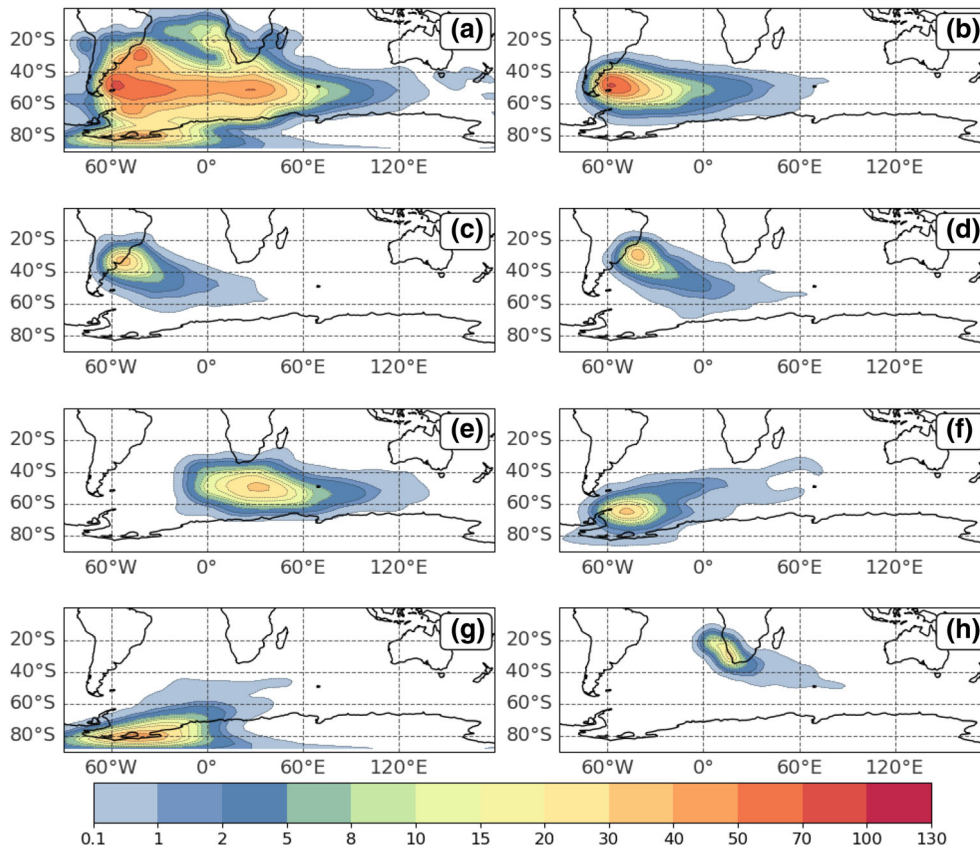


**FIGURE 6** Cyclone track density for intensification phase for austral summer (DJF) (a) for all systems with genesis in the South Atlantic, (b) for ARG, (c) for LA-PLATA, (d) for SE-BR, (e) for SE-SAO, (f) for AT-PEN, (g) for WEDDELL, (h) for SA-NAM. The track density unit is cyclone per  $10^6 \text{ km}^2$  per month. [Colour figure can be viewed at [wileyonlinelibrary.com](http://wileyonlinelibrary.com)]

seasonality observed here aligns with previous studies (Crespo et al., 2021; Gan & Rao, 1991; Gramcianinov et al., 2019; Hoskins & Hodges, 2005; Mendes et al., 2010; Reboita et al., 2010a).

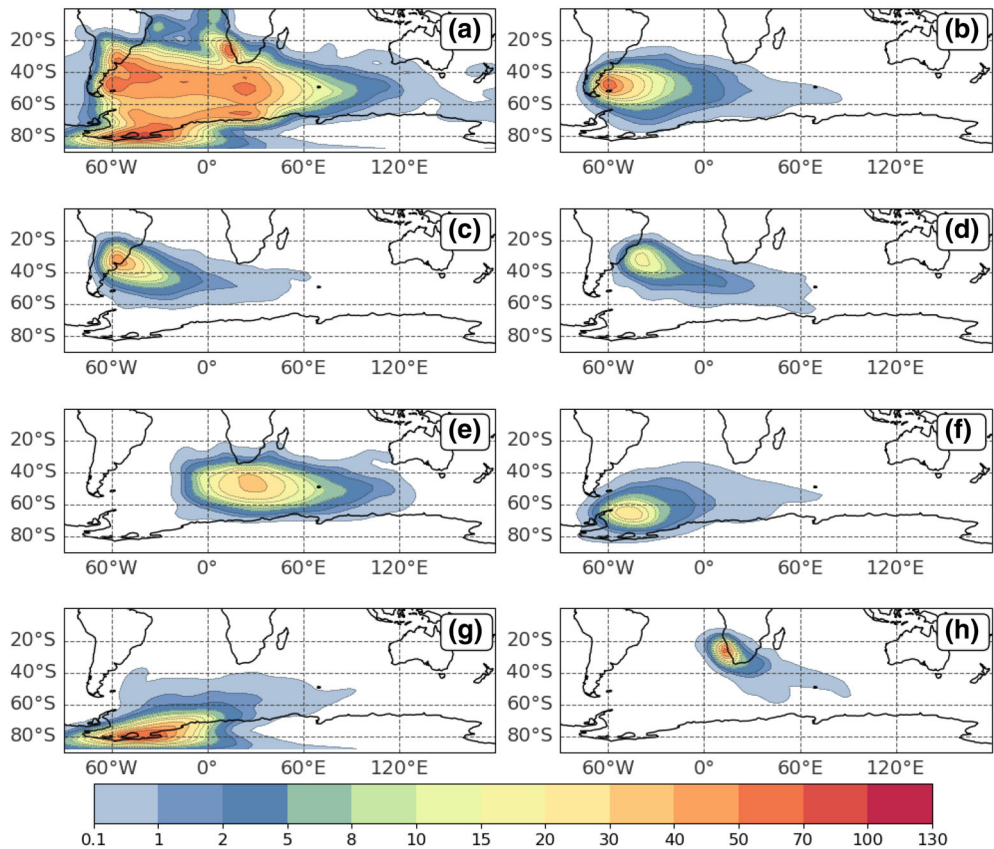
The SE-SAO region exhibits increased activity during JJA (Figure 5b) compared to DJF (Figure 5a), with densities for the incipient stage exceeding 10 and 5 cyclones per  $10^6 \text{ km}^2$  per month, respectively. Notably, this region demonstrates a wider spatial distribution of density than the others, with DJF tracks resembling a continuous area of incipient systems extending from the ARG region to the western boundary of the SAt. Track densities related to WEDDELL and SA-NAM regions are also more prominent during JJA than DJF, exceeding 15 cyclones per  $10^6 \text{ km}^2$  per month. During DJF, WEDDELL experiences genesis at a rate of up to 10 cyclones per  $10^6 \text{ km}^2$  per month, while the SA-NAM region's genesis is nearly negligible, merging with the SE-SAO region. In contrast, SAT-PEN presents similar densities and spatial patterns for both seasons, with maximum densities close to 10 and 8 cyclones per  $10^6 \text{ km}^2$  per month for JJA and DJF, respectively.

### 3.3.2 | Intensification phase

In the intensification phase (Figures 6 and 7), the track densities exhibit significantly higher values than the

incipient stage, as expected due to the longer duration of the intensification phase (refer to Figure 1). During DJF and JJA, the track densities range from approximately 60°E to 60°W, with a central concentration around 50°S. Notably, there is an area of maximum density east of ARG during both seasons. During DJF (Figure 6d), this maximum density region displays higher densities (reaching 70 cyclones per  $10^6 \text{ km}^2$  per month) and is oriented southeastward in relation to the maximum density region observed during the incipient stage. Furthermore, during DJF, there is a separate maximum track density region associated with SE-BR, as shown in Figure 6. This SE-BR region also displays southeastward orientation, with densities reaching up to 40 cyclones per  $10^6 \text{ km}^2$  per month, and it is centred in a region close to the incipient maximum. This implies that the systems generated in the SE-BR region tend to intensify near their genesis area and exhibit relatively low mobility during the intensification phase. However, it is important to note that, for this season, while LA-PLATA presents maximum track densities comparable to SE-BR, the LA-PLATA region does not appear as distinctly in the densities map when considering all systems (Figure 6). This is because LA-PLATA is oriented southeastward and is thus overshadowed by the ARG tracks. In JJA, the intensification stage reveals a maximum track density extending from LA-PLATA to its southeast (Figure 7c) and another region that stretches

**FIGURE 7** Same as Figure 6, but for austral winter (JJA). [Colour figure can be viewed at [wileyonlinelibrary.com](http://wileyonlinelibrary.com)]



from ARG to the east (Figure 7d), with both regions exceeding 50 cyclones per  $10^6 \text{ km}^2$  per month. These two regions are interconnected (Figure 7a). This pattern indicates that while ARG cyclones exhibit distinct displacements for DJF and JJA during the intensification stage, the systems originating at LA-PLATA tend to present similar displacements across seasons.

SE-SAO displays a comparable behaviour for both DJF and JJA (Figures 6e and 7e), with the latter exhibiting higher track density, in line with increased genesis activity during this period (Gramcianinov et al., 2019). In DJF, a maximum density region exceeding 50 cyclones per  $10^6 \text{ km}^2$  per month is situated southeastward of the region of maximum density for the incipient stage, centred near  $30^\circ\text{E}$  and  $50^\circ\text{S}$ . For JJA, this region shifts eastward of the genesis region, centred near  $20^\circ\text{E}$  and  $45^\circ\text{S}$ . This positioning relative to the genesis region implies that these systems undergo either high mobility during the intensification stage or experience prolonged intensification periods. Similar to the ARG region, there is a seasonality in the displacement of these systems during the intensification stage. In DJF, when looking for all systems generated in the South Atlantic (Figure 6), close to  $15^\circ\text{E}$ , two centres of maximum density exceeding 50 cyclones per  $10^6 \text{ km}^2$  per month are observed, one at  $50^\circ\text{S}$  and the other at  $70^\circ\text{S}$ . While the former can be attributed to the SE-SAO region, the latter cannot be associated with any specific genesis

region, most likely resulting from the superposition of systems from various regions intensifying in this area.

Furthermore, a maximum track density region exceeding 30 cyclones per  $10^6 \text{ km}^2$  per month appears southeast of the AT-PEN, connected to the maximum density region originating from the WEDDELL genesis area (with densities above 40 cyclones per  $10^6 \text{ km}^2$ ) per month and extending to the northeast. In contrast to the incipient stage, maximum densities for AT-PEN are higher during DJF than JJA (35 and 30 cyclones per  $10^6 \text{ km}^2$  per month, respectively), suggesting that systems in DJF exhibit smaller displacements compared to those in JJA. During JJA, the maximum density region indicates an eastward displacement, while DJF suggests a northeastward shift. The WEDDELL region presents similar density patterns for both DJF and JJA, with higher densities during JJA, consistent with the pattern indicated by the incipient stage. Lastly, albeit more active during JJA, densities near SA-NAM remain concentrated around the density region observed in the incipient stage, indicating that these systems exhibit lower mobility.

### 3.3.3 | Mature phase

For the mature stage, the track density representing all the systems generated in the South Atlantic exhibits a

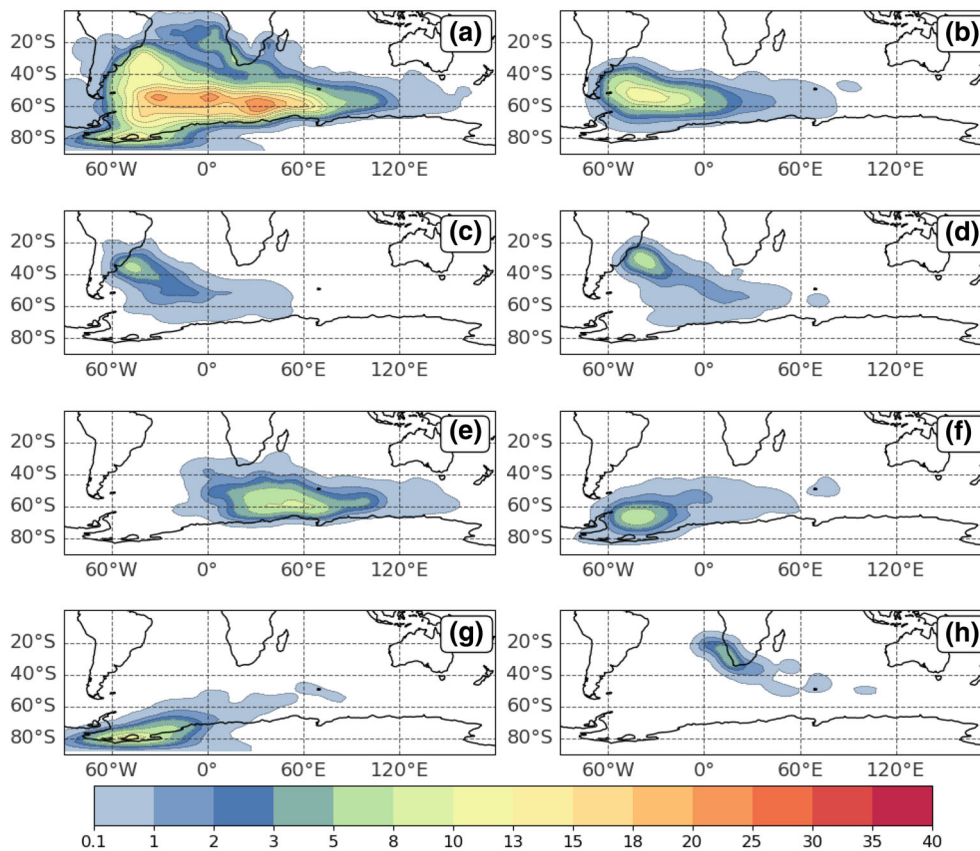


**FIGURE 8** Same as Figure 6, but for mature phase.  
[Colour figure can be viewed at [wileyonlinelibrary.com](http://wileyonlinelibrary.com)]

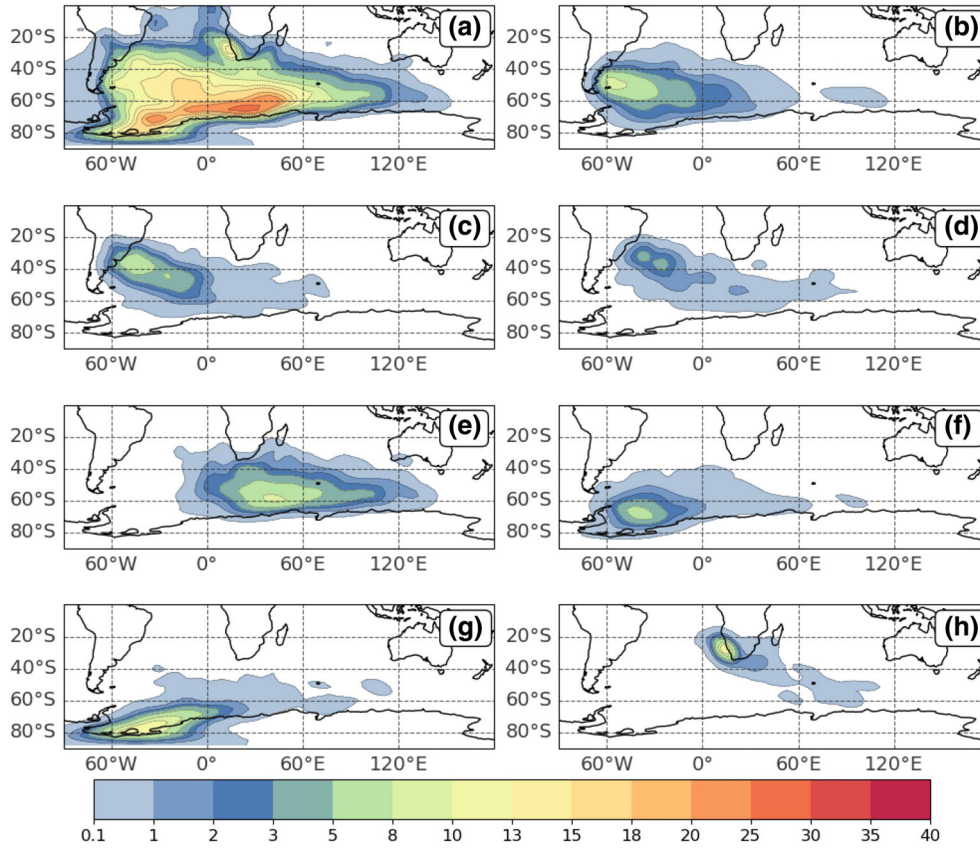


**FIGURE 9** Same as Figure 6, but for mature phase and for austral winter (JJA).  
[Colour figure can be viewed at [wileyonlinelibrary.com](http://wileyonlinelibrary.com)]

spatial pattern shifted southeastward from the intensification stage's densities (Figures 8a and 9a), with a maximum density region centred at 20°E and 65°S. This pattern closely resembles the spatial structure of Southern Atlantic storm tracks, albeit with the maximum density region positioned further south (Gramcianinov et al., 2019; Hoskins & Hedges, 2005). During DJF, three spots of maximum track densities become apparent. The first, situated around 30°W and 55°S, can be attributed to the convergence of mature systems from the genesis regions along the South American coast, SE-BR, LA-PLATA and ARG (Figure 8a–c, respectively). The second spot, located approximately at 0° and 55°S, likely results from the overlapping of systems originating from the South American coast, less mobile systems from SE-SAO (Figure 8e) and highly mobile systems from WEDDELL (Figure 8g). The last maximum, centred at 30°E and 60°S, is situated southeast of the region with the highest density during the intensification period, including systems with genesis across all regions within the study area, especially SE-SAO. Meanwhile, during JJA, two regions of maximum densities emerge. The first, located between 30°S and 70°S, is associated with AT-PEN and WEDDELL regions (Figure 9f,g). The second region, spanning from 10°W to 50°E and centred at approximately 65°S, represents the maturation of systems from all the genesis regions within the study area. Notably, there is a secondary maximum in the SA-NAM region, confirming the low mobility of these systems.

The ARG region exhibits a distinct seasonality in the spatial pattern of maximum density associated with the mature stage. During DJF, a maximum density region exceeding 10 cyclones per  $10^6 \text{ km}^2$  per month emerges southeastward of the region related to the intensification stage (Figure 8b). In contrast, during JJA (Figure 9b), there is a region with a maximum track density exceeding 8 cyclones per  $10^6 \text{ km}^2$  per month, positioned eastward the areas of maximum track densities for the intensification and incipient stages. On the other hand, the LA-PLATA and SE-BR regions present a maximum track density that does not exceed 8 cyclones per  $10^6 \text{ km}^2$  per month (Figures 8c,d and 9c,d). For DJF, cyclones originating from both regions commence their maturation southeastward from the maximum track density associated with the intensification stage, extending up to 50°E. During JJA, LA-PLATA systems mature up to 70°E, while SE-BR exhibits lower maximum track densities, not exceeding 5 cyclones per  $10^6 \text{ km}^2$  per month, which aligns with the lower activity of this region during this season.

For the systems with genesis in the SE-SAO region, a maximum track density exceeding 8 cyclones per  $10^6 \text{ km}^2$  per month is centred at 60°S and 40°E during

DJF and 50°E during JJA (Figure 9e). Cyclones from this region mature from the area close to the genesis maximum, extending up to the southeastern boundary of the Indian Ocean. The AT-PEN region demonstrates consistent spatial patterns for both seasons, with a maximum track density exceeding 8 cyclones per  $10^6 \text{ km}^2$  per month centred at 40°W and 65°S (Figures 8f and 9f). Systems originating in this region mature from 70°W to the southeastern Indian Ocean. WEDDELL region exhibits maximum track densities exceeding 10 cyclones per  $10^6 \text{ km}^2$  per month for both seasons (Figures 8g and 9g). During DJF, this maximum density region closely aligns with that of the incipient phase. However, during JJA, the region expands northeastward, similar to the intensification stage. In the SA-NAM region, during DJF, the densities are almost negligible, not exceeding 5 cyclones per  $10^6 \text{ km}^2$  per month. In contrast, during JJA, systems display a maximum track density exceeding 10 cyclones per  $10^6 \text{ km}^2$  per month concentrated over the same area as the incipient and intensification stages (Figure 9g). This reaffirms the stationary nature of these systems.

### 3.3.4 | Decay phase

The decay stage exhibits the highest track densities among all phases of the cyclone life cycle for both DJF and JJA when considering all cyclones with genesis in the South Atlantic (Figures 10a and 11a). In both seasons, the maximum track density surpasses 100 cyclones per  $10^6 \text{ km}^2$  per month and is centred at 65°S and 30°W. Cyclones in the decay stage disperse throughout the entire South Atlantic, extending as far as the southeastern boundary of the Indian Ocean. These results are aligned with Sinclair (1995). As with previous phases, the systems with genesis in the ARG region exhibits a distinct seasonal pattern, with maximum track densities exceeding 20 cyclones per  $10^6 \text{ km}^2$  per month in both seasons (Figures 10b and 11b). In DJF, this maximum density region spans from 50°W to 20°E, suggesting either higher mobility or longer decay periods during this season. In contrast, in JJA, it is centred southeast of the peak density observed during the intensification stage. The systems with genesis at LA-PLATA exhibits maximum track densities for both seasons that exceed 15 cyclones per  $10^6 \text{ km}^2$  per month (Figures 10c and 11c). The track density regions are centred in the same area observed in the mature stage but extend further southeastward and northwestward. The density to the northwest aligns with the maximum density related to the incipient stage, representing systems that undergo early decay (Figure 2). During JJA, the maximum track density region extends over a larger area, in alignment with the increased

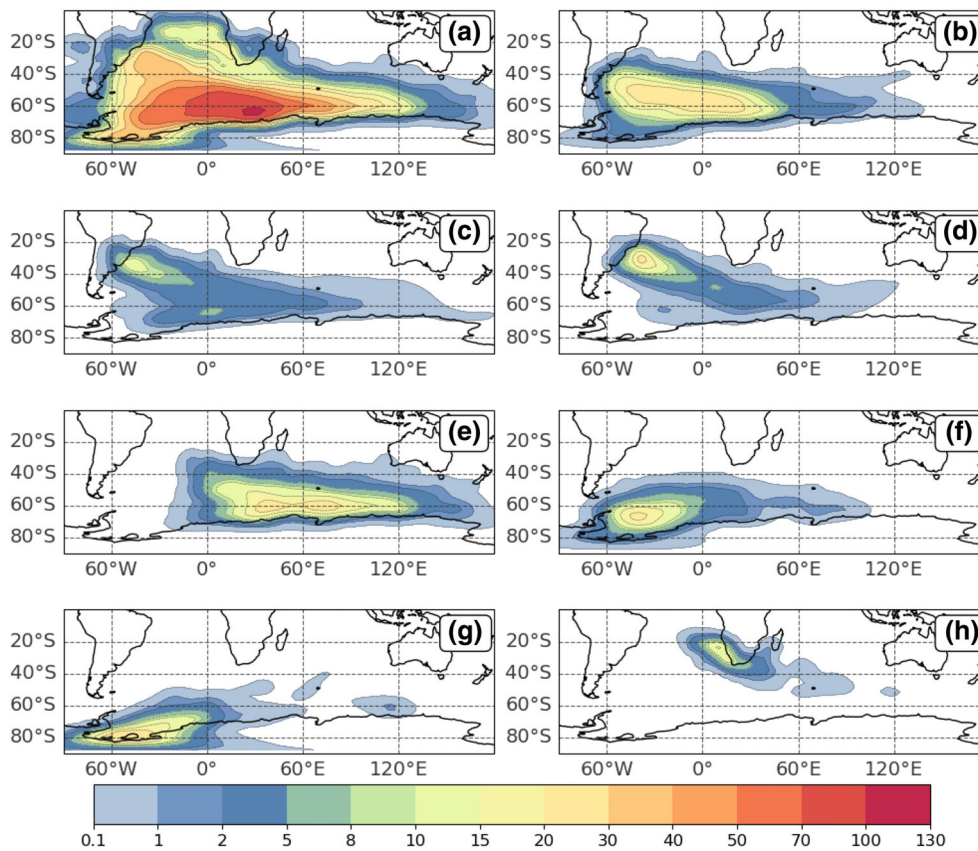


**FIGURE 10** Same as Figure 6, but for decay phase.  
[Colour figure can be viewed at [wileyonlinelibrary.com](http://wileyonlinelibrary.com)]

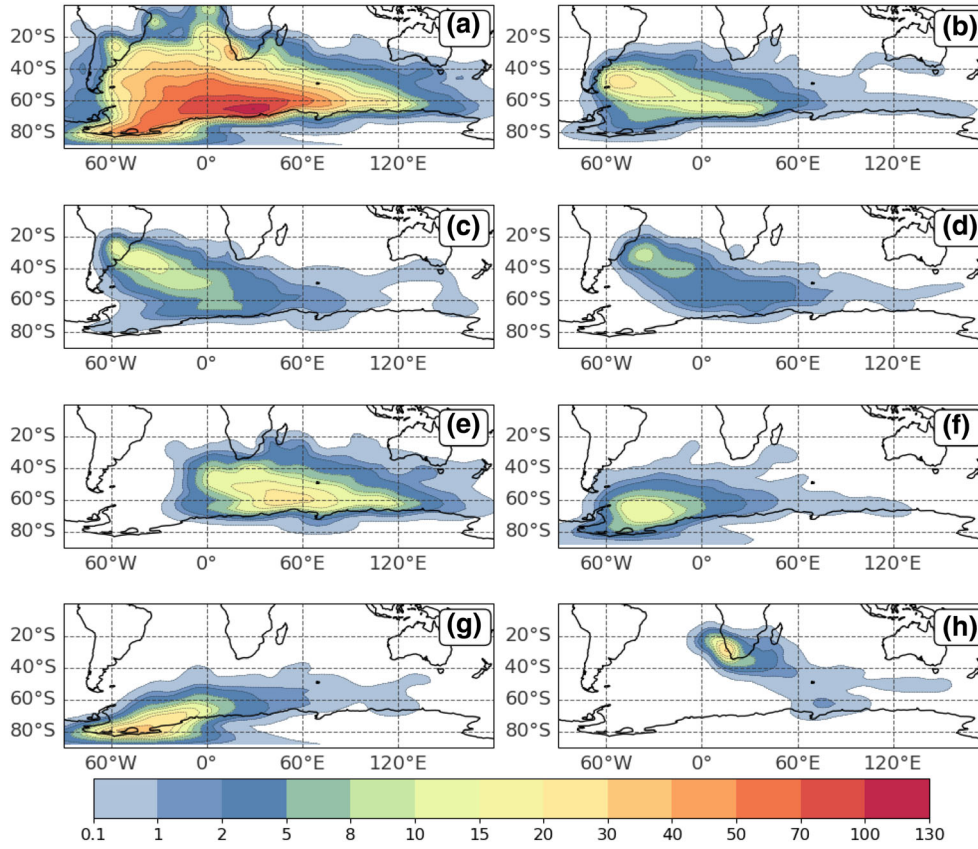
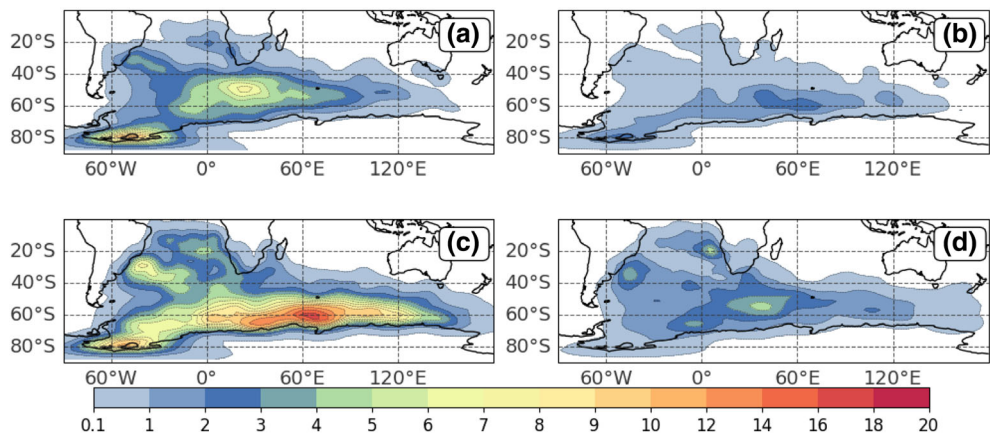


**FIGURE 11** Same as Figure 6, but for mature phase and for austral winter (JJA).  
[Colour figure can be viewed at [wileyonlinelibrary.com](http://wileyonlinelibrary.com)]

**FIGURE 12** Cyclone track density for secondary development phases (a–c) for austral summer (DJF) and residual (d). (a) Second intensification stage, (b) second mature stage, (c) second decay stage. The track density unit is cyclone per  $10^6 \text{ km}^2$  per month. [Colour figure can be viewed at [wileyonlinelibrary.com](http://wileyonlinelibrary.com)]



genesis activity during this season. SE-BR also displays a maximum track density near the regions observed in previous phases, underscoring the limited mobility of these systems (Figures 10d and 11d). The maximum track density exceeds 20 and 8 cyclones per  $10^6 \text{ km}^2$  per month for JJA and DJF, respectively, highlighting the increased activity of this region during DJF.

Despite its seasonal activity for genesis, SE-SAO presents similar patterns for both DJF and JJA for the decay stage, presenting a maximum track density east of the one for the mature stage, exceeding 20 cyclones per  $10^6 \text{ km}^2$  per month (Figures 8e and 9e). Notably, some systems with genesis in this region decay farther east, on the southwestern Pacific Ocean. SAT-PEN systems decay close to their maturation, with maximum track densities centred at  $40^\circ\text{E}$  and  $65^\circ\text{S}$  (Figures 8f and 9f). However, during DJF, the maximum track density is notably higher than for JJA (exceeding 30 and 10 cyclones per  $10^6 \text{ km}^2$  per month, respectively). This indicates that SAT-PEN systems present longer decay during DJF. Meanwhile, WEDDELL presents the same spatial pattern as for previous stages (Figures 8g and 9g). For this region, the maximum track density is closer to the maximum density of incipient, intensification and mature phases during DJF, while JJA maximum density is oriented northeastward (exceeding 20 and 30 cyclones per  $10^6 \text{ km}^2$  per month, respectively). Lastly, SA-NAM presents the same pattern present for previous stages, with systems close to the genesis region and decreased activity for DJF when compared to JJA, with systems exceeding 10 and 15 cyclones per  $10^6 \text{ km}^2$  per month, respectively (Figures 8h and 9h).

### 3.3.5 | Secondary development stages

Figures 12 and 13 show the secondary development stages (including a second intensification, mature and/or

decay phases) during DJF and JJA, respectively, for Southern Atlantic-originating systems. Track density for these stages is lower, indicating that only a subset of systems experience secondary development, as illustrated in Figure 2.

The second intensification stage shows two distinct density maxima. The first, near  $50^\circ\text{S}$  and  $30^\circ\text{E}$  during DJF (Figure 12a), is close to the SE-SAO cyclogenesis region and shows a higher track density, surpassing 8 cyclones per  $10^6 \text{ km}^2$  per month. In JJA (Figure 13a), this maximum does not have a cohesive spatial structure and is spread from approximately  $40^\circ\text{S}$  to  $70^\circ\text{S}$  and from  $0^\circ$  to  $60^\circ\text{E}$ , with densities ranging from 4 to 6 cyclones per  $10^6 \text{ km}^2$  per month. The second density maximum, near the decay maxima for the WEDDELL region for both seasons, shows higher densities in DJF than JJA (exceeding 12 and 8 cyclones per  $10^6 \text{ km}^2$  per month, respectively). This is a notable contrast to the mature stage, where JJA typically presents higher track densities. This pattern suggests a non-negligible proportion of systems originating from the WEDDELL region undergo secondary development, particularly in DJF.

Gramcianinov et al. (2019) highlighted a potential link between the SE-SAO region and secondary cyclogenesis. We do not exclude the possibility of some of the detected re-intensification might stem from secondary cyclogenesis events or spurious links by the TRACK algorithm, mixing weak decaying systems with incipient secondary cyclones. This necessitates further investigation, especially since re-intensification near the WEDDELL region aligns with growth regions identified by Hoskins and Hodges (2005), suggesting these instances are more likely re-intensifications than new cyclogenesis events, underscoring the need for additional climatological research on WEDDELL-origin systems.

While secondary cyclogenesis generally follows a frontal wave post an extratropical cyclone's passage (Ford et al., 1990; Mailier et al., 2006; Rivals et al., 1998;

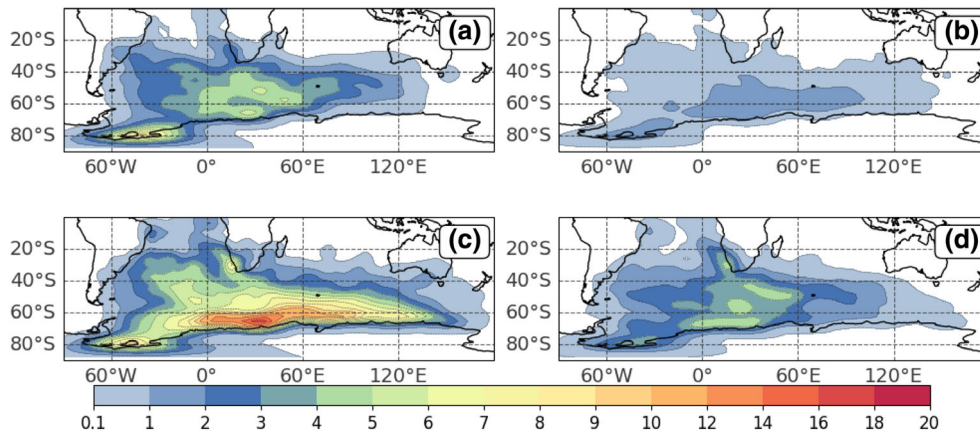


**FIGURE 13** Same as Figure 12 but for austral winter (JJA). [Colour figure can be viewed at [wileyonlinelibrary.com](http://wileyonlinelibrary.com)]

Shapiro et al., 1997), the CycloPhaser identifies a unique pattern of secondary development involving re-intensification and subsequent mature and decay phases. This secondary intensification could result from a decaying wave at 850 hPa finding favourable conditions or, if the surface cyclone has dissipated and the TRACK algorithm is tracking a weak through at 850 hPa, the CycloPhaser may classify this weak intensification as “residual” should it not progress to a mature stage. Conversely, if the TRACK algorithm mistakenly associates this decaying wave with a newly forming cyclone nearby, the CycloPhaser labels the transition as “re-intensification,” introducing potential analysis errors. However, distinguishing between true secondary genesis and re-intensification remains beyond this study’s scope.

The second mature stage exhibits the lowest maximum density among the secondary development stages, aligning with its shortest mean duration in the entire life cycle (Figure 4b). During DJF (Figure 12b), the maximum density is higher than in JJA (Figure 13b), exceeding 1 and 2 cyclones per  $10^6 \text{ km}^2$  per month, respectively. This maximum density region contours the Antarctic coastline, extending from the WEDDELL genesis area at approximately 90°E and positioned southeast of the maxima observed for the second intensification stage.

For the second decay stage, two distinct density maxima are observed. The first, exhibiting higher densities, is located eastward of the mature stage maxima during DJF, near 60°E and 60°S, with densities surpassing 16 cyclones per  $10^6 \text{ km}^2$  per month (Figure 12c). During JJA, this centre shifts southward of the SE-SAO genesis region, near 30°E and 60°S (Figure 13c). Notably, this centre of maximum second decay is positioned westward of the first decay stage’s maxima. It is associated with systems originating in SE-SAO that followed distinct trajectories compared to those undergoing only a single developmental stage, systems from WEDDELL, and highly mobile systems from the genesis regions along the

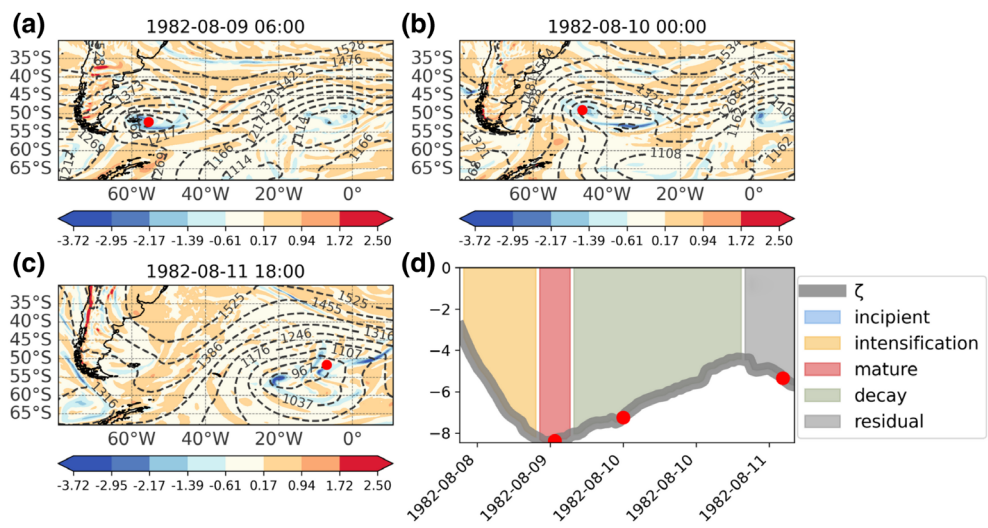
South American coast. The second centre, located near the WEDDELL genesis region, exhibits higher densities in DJF than in JJA (exceeding 12 and 8 cyclones per  $10^6 \text{ km}^2$  per month, respectively). This pattern suggests limited mobility for WEDDELL systems undergoing secondary development.

A notable observation in both the second intensification and decay phases is the region near the SE-BR genesis area during DJF, where relatively high track densities extend southwestward. While a significant proportion of systems decaying in this region may be associated with early decay in their life cycle 2, other processes should also be considered. This region is known for the occurrence of subtropical cyclones during DJF (Cardoso et al., 2022; de Jesus et al., 2022; Evans & Braun, 2012), with approximately 30% of the systems exhibiting hybrid characteristics (Gozzo et al., 2014). Case studies of such systems originating in the SE-BR region reveal complex life cycles, often transitioning between different system types and presenting multiple stages of intensification, maturation and decay (e.g., Dias Pinto et al., 2013; Dutra et al., 2017; Reboita et al., 2021; Reboita et al., 2022; Veiga et al., 2008). Consequently, it is plausible that some of the systems represented in these high-density areas might be subtropical. However, further analysis is needed to confirm this hypothesis.

### 3.3.6 | Residual

The residual phase, although not indicative of a physical cyclone development stage per se, is crucial for understanding tracking and detection discrepancies, and it suggests areas for methodological refinement. This phase primarily captures systems that undergo temporary intensification due to favourable environmental conditions but do not evolve into mature cyclones. Detection of the residual phase involves recognizing instances

**FIGURE 14** Relative vorticity (shaded) and geopotential heights (contours) at 850 hPa illustrate the mature (a) and decaying (b) stages of a representative system that exhibits a residual phase in its life cycle (c). The complete life cycle of the system is depicted in (d). [Colour figure can be viewed at [wileyonlinelibrary.com](http://wileyonlinelibrary.com)]



where a system's central vorticity increases outside the typical development cycle, often influenced by proximity to other systems or localized atmospheric conditions conducive to intensification.

During DJF, significant track densities for residuals are noted in SE-BR, SA-NAM and SE-SAO regions. Cyclones from SE-BR, often weaker and lacking closed isobars (Hoskins & Hodges, 2005; Sinclair, 1995), might experience residual intensification near the Brazil-Malvinas confluence, an area fostering low-level baroclinicity (Gordon, 1989; Sanders & Gyakum, 1980). This suggests that residuals may represent weak systems briefly intensifying due to favourable conditions but not achieving maturity. For SA-NAM and SE-SAO, despite limited research, the SE-SAO's maxima's positioning indicates that upper-level jet support (e.g., Swart et al., 2015) and baroclinic environments (e.g., Hoskins & Hodges, 2005) could similarly drive marginal intensification, leading to a residual classification.

Conclusive statements for dynamics associated with the residual from regions like SA-NAM is hindered by scarce research. Yet, SE-SAO's maxima during DJF and JJA (Figure 13d), positioned south of the upper-level jet's mean location (e.g., Swart et al., 2015), imply upper-level jet support might spur marginal intensification, categorizing as residual. Notably, SA-NAM's maximum track density exhibits seasonal shifts, moving northwest in DJF and south in JJA (Figures 12d and 13d), reflecting seasonal dynamic variations influencing residual classifications in SA-NAM-origin cyclones.

Figure 14 illustrates the emergence of a residual phase. Initially, Figure 14a presents a mature cyclone with closed isobars at 850 hPa. However, Figure 14b reveals the system entering decay, with open isobars and diminished relative vorticity cohesion. A nearby system influences the decaying system, intensifying its central

relative vorticity (Figure 14c), indicating temporary re-intensification. Eventually, the TRACK algorithm discontinues the tracking, signifying the end of observation (Figure 14d). This process of transitory intensification following the decay stage is not related to the original system's life cycle and thus is classified as residual.

#### 4 | SUMMARY AND CONCLUDING REMARKS

This study introduces CycloPhaser, a novel, open-source Python package for automated cyclone life cycle detection, available on PyPI repository. Its low memory footprint, flexibility and rapid deployment capabilities make it a valuable asset for climatological studies or even operational forecasts. The research identified a total of 33,376 systems from 1979 to 2020, focusing on configurations that accounted for at least 1% of the overall life cycle types count and presented at least one mature phase. These represented approximately 95% of the total systems, amounting to 31,719 systems in total. The most common cyclone type followed a four-phase configuration: incipient, intensification, mature and decay, accounting for about 60% of the analysed systems. The results from the CycloPhaser program align well with previous studies regarding cyclone behaviour in the South Atlantic region, confirming known cyclogenesis regions and providing statistical insights into cyclone lifetimes and paths. The CycloPhaser program calculated an average cyclone lifetime of approximately 90.72 h (3.78 days) and an average displacement of 3269 km, findings that largely corroborate those of previous studies and indicate a broad range of cyclone behaviours.

The research presents a detailed analysis of South Atlantic cyclone development stages, including incipient,

intensification, mature, decay and secondary development. The incipient phase primarily occurs in established cyclogenesis regions along the South American coast (SE-BR, LA-PLATA and ARG), with additional regions identified in the Southeast Atlantic, near South Africa and Namibia (SA-NAM), the Antarctic Peninsula (AT-PEN), and the Weddell Sea (WEDDELL). These regions show seasonal variations, being most active during JJA, except SE-BR, which peaks in DJF, and ARG, showing little seasonal change. The intensification phase reveals high track densities near 50°S, primarily east or southeast of genesis regions, except for WEDDELL, where tracks are denser northwest of the genesis, and SA-NAM, which displays stationary behaviour. This displacement pattern is consistent in the remaining phases. The mature phase tracks converge near Antarctica's coast at approximately 70°S, 30°E, while the decay phase shows a broader spread, reflecting the high mobility and early decay of some systems. Both mature and decay phases exhibit noticeable seasonality, shifting south/southeastward during JJA. Secondary development stages are less dense but show significant seasonal variability. Also, the importance of the WEDDELL region for secondary life cycle occurrence is highlighted, while acknowledging the limitations in fully understanding this aspect due to the scarcity of existing research.

The results presented here contribute significantly to the climatology of South Atlantic cyclones by enabling a more comprehensive exploration of neglected or less-studied regions. By identifying and including additional cyclogenesis regions like SE-SAO, SA-NAM, AT-PEN and the WEDDELL, the climatology presented here opens up new avenues for understanding cyclone formation and behaviour in these areas. This expanded focus is crucial for a more complete understanding of the climatological patterns and variations in cyclone activity across SAt. Furthermore, the CycloPhaser's detailed analysis of cyclone life cycle types, particularly the focus on configurations accounting for significant proportions of cyclone activity, enhances our understanding of the spatial distribution of cyclone phases. This analysis not only reaffirms the common four-phase configuration (incipient, intensification, mature and decay) but also sheds light on variations in cyclone development cycles, thereby contributing to a better understanding of how different regions within SAt influence the formation and evolution of distinct cyclone types. These insights are valuable for improving weather forecasting and developing effective mitigation strategies in the region.

While the CycloPhaser program provides a novel and effective tool for analysing cyclone life cycles in the South Atlantic, it is important to acknowledge this study's limitations. The analysis at this single atmospheric level,

offers a concentrated but partial view of cyclone life cycle. Consequently, our conclusions about cyclone characteristics through their life cycle predominantly reflect the processes observable at the 850 hPa level. This methodological choice inherently limits our ability to fully explore the cyclones' vertical development and the complex interactions occurring at different atmospheric altitudes. Future research could benefit from incorporating a multi-level approach, providing a more holistic understanding of cyclone dynamics across the troposphere.

One of the unique contributions of this research is the assessment of cyclone life cycle stages along their storm tracks, a perspective not commonly explored in existing cyclone track climatologies. This approach may open avenues for future research, particularly in understanding the nuances of cyclone development mechanisms and behaviour. From this first application, several open questions popped-up, highlighting the complexity and dynamic nature of cyclone systems. Using the method presented here, future studies can investigate further the primary processes associated with each development stage in the life cycles of cyclones, including the secondary development stages reported herein—and if some of these cases configure a secondary genesis instead.

## AUTHOR CONTRIBUTIONS

**Danilo Couto de Souza:** Conceptualization; methodology; software; validation; investigation; formal analysis; data curation; visualization; writing – original draft. **Pedro Leite da Silva Dias:** Validation; resources; writing – review and editing; supervision; funding acquisition. **Carolina Barnez Gramcianinov:** Investigation; data curation; writing – review and editing. **Matheus Bonjour Laviola da Silva:** Resources; writing – review and editing. **Ricardo de Camargo:** Resources; supervision; funding acquisition.

## ACKNOWLEDGEMENTS

This study was partly financed by the Coordenação de Aperfeiçoamento de Pessoal de Nível Superior-Brasil (CAPES) under Finance Code 001. CBG is funded by the Helmholtz European Partnership “Research Capacity Building for Healthy, Productive and Resilient Seas” (SEA-ReCap, Grant No. PIE-0025). The first author to the Laboratory of Applied Meteorology for Regional Meteorological Systems (MASTER) for the data processing infrastructure, special thanks are extended to Jean Peres and Djalma Vieira for their invaluable technical assistance and support in the laboratory, contributing significantly to the success of this research.

## CONFLICT OF INTEREST STATEMENT

The authors declare no conflicts of interest.

## DATA AVAILABILITY STATEMENT

The cyclone tracks used in this study were obtained from the "Atlantic extratropical cyclone tracks database" (<https://doi.org/10.17632/kwcvfr52hp.4>). The CycloPhaser code is available at <https://pypi.org/project/cyclophaser>.

## ORCID

Danilo Couto de Souza  <https://orcid.org/0000-0003-4121-7583>

Pedro Leite da Silva Dias  <https://orcid.org/0000-0002-4051-2962>

Carolina Barnez Gramcianinov  <https://orcid.org/0000-0002-3919-5226>

Matheus Bonjour Laviola da Silva  <https://orcid.org/0000-0002-8629-8762>

Ricardo de Camargo  <https://orcid.org/0000-0002-9425-5391>

## REFERENCES

- Acevedo, O.C., Pezzi, L.P., Souza, R.B., Anabor, V. & Degrazia, G.A. (2010) Atmospheric boundary layer adjustment to the synoptic cycle at the Brazil-Malvinas confluence, South Atlantic Ocean. *Journal of Geophysical Research: Atmospheres*, 115, D22107.
- Azad, R. & Sorteberg, A. (2014) The vorticity budgets of North Atlantic winter extratropical cyclone life cycles in MERRA reanalysis. Part I: development phase. *Journal of the Atmospheric Sciences*, 71, 3109–3128.
- Bengtsson, L., Hodges, K.I. & Keenlyside, N. (2009) Will extratropical storms intensify in a warmer climate? *Journal of Climate*, 22, 2276–2301.
- Bjerknes, J. (1922) Life cycle of cyclones and the polar front theory of atmospheric circulation. *Geophys. Publ.*, 3, 1–18.
- Booth, J.F., Naud, C.M. & Jeyaratnam, J. (2018) Extratropical cyclone precipitation life cycles: a satellite-based analysis. *Geophysical Research Letters*, 45, 8647–8654.
- Campos, R.M., Camargo, R.D. & Harari, J. (2010) Characterization of extreme sea level events in Santos and their correspondence with the NCEP model reanalysis in the southwest of the South Atlantic. *Revista Brasileira de Meteorologia*, 25, 175–184.
- Cardoso, A.A., da Rocha, R.P. & Crespo, N.M. (2022) Synoptic climatology of subtropical cyclone impacts on near-surface winds over the South Atlantic basin. *Earth and Space Science*, 9, e2022EA002482.
- Carrasco, J.F., Bromwich, D.H. & Monaghan, A.J. (2003) Distribution and characteristics of mesoscale cyclones in the Antarctic: Ross Sea eastward to the Weddell Sea. *Monthly Weather Review*, 131, 289–301.
- Crespo, N.M., da Rocha, R.P., Sprenger, M. & Wernli, H. (2021) A potential vorticity perspective on cyclogenesis over centre-eastern South America. *International Journal of Climatology*, 41, 663–678.
- Crespo, N.M., Reboita, M.S., Gozzo, L.F., de Jesus, E.M., Torres-Alavez, J.A., Lagos-Zúñiga, M.Á. et al. (2023) Assessment of the RegCM4-CORDEX-CORE performance in simulating cyclones affecting the western coast of South America. *Climate Dynamics*, 60, 2041–2059.
- Da, C., Shen, B., Yan, P., Ma, D. & Song, J. (2017) The shallow water equation and the vorticity equation for a change in height of the topography. *PLoS One*, 12, e0178184.
- Dacre, H.F. & Gray, S.L. (2009) The spatial distribution and evolution characteristics of North Atlantic cyclones. *Monthly Weather Review*, 137, 99–115.
- de Jesus, E.M., da Rocha, R.P., Crespo, N.M., Reboita, M.S. & Gozzo, L.F. (2022) Future climate trends of subtropical cyclones in the South Atlantic basin in an ensemble of global and regional projections. *Climate Dynamics*, 58, 1221–1236.
- de Souza, D. & da Silva, R.R. (2021) Ocean-land atmosphere model (OLAM) performance for major extreme meteorological events near the coastal region of southern Brazil. *Climate Research*, 84, 1–21.
- Dias Pinto, J.R., Reboita, M.S. & da Rocha, R.P. (2013) Synoptic and dynamical analysis of subtropical cyclone Anita (2010) and its potential for tropical transition over the South Atlantic Ocean. *Journal of Geophysical Research: Atmospheres*, 118, 10–870.
- Duchon, C.E. (1979) Lanczos filtering in one and two dimensions. *Journal of Applied Meteorology and Climatology*, 18, 1016–1022.
- Dutra, L.M.M., da Rocha, R.P., Lee, R.W., Peres, J.R.R. & de Camargo, R. (2017) Structure and evolution of subtropical cyclone Anita as evaluated by heat and vorticity budgets. *Quarterly Journal of the Royal Meteorological Society*, 143, 1539–1553.
- Evans, J.L. & Braun, A. (2012) A climatology of subtropical cyclones in the South Atlantic. *Journal of Climate*, 25, 7328–7340.
- Flaounas, E., Kotroni, V., Lagouvardos, K. & Flaounas, I. (2014) Cyclotrack (v1.0)—tracking winter extratropical cyclones based on relative vorticity: sensitivity to data filtering and other relevant parameters. *Geoscientific Model Development*, 7, 1841–1853.
- Ford, R., Ford, R.P., Moore, G.W.K., Moore, G.W.K. & Moore, G.W.K. (1990) Secondary cyclogenesis—comparison of observations and theory. *Monthly Weather Review*, 118, 427–446.
- Gan, M.A. & Rao, V.B. (1991) Surface cyclogenesis over South America. *Monthly Weather Review*, 119, 1293–1302.
- Gan, M.A. & Rao, V.B. (1994) The influence of the Andes Cordillera on transient disturbances. *Monthly Weather Review*, 122, 1141–1157.
- Gordon, A.L. (1989) Brazil-Malvinas confluence—1984. *Deep Sea Research Part A: Oceanographic Research Papers*, 36, 359–384.
- Gozzo, L., Da Rocha, R., Gimeno, L. & Drumond, A. (2017) Climatology and numerical case study of moisture sources associated with subtropical cyclogenesis over the southwestern Atlantic Ocean. *Journal of Geophysical Research: Atmospheres*, 122, 5636–5653.
- Gozzo, L.F., da Rocha, R.P., Reboita, M.S. & Sugahara, S. (2014) Subtropical cyclones over the southwestern South Atlantic: climatological aspects and case study. *Journal of Climate*, 27, 8543–8562.
- Gramcianinov, C., Campos, R., De Camargo, R., Hodges, K., Soares, C.G. & da Silva Dias, P. (2020a) Analysis of Atlantic extratropical storm tracks characteristics in 41 years of ERA5 and CFSR/CFSV2 databases. *Ocean Engineering*, 216, 108–111.
- Gramcianinov, C., Hodges, K. & Camargo, R.D. (2019) The properties and genesis environments of South Atlantic cyclones. *Climate Dynamics*, 53, 4115–4140.

- Gramcianinov, C.B., Campos, R.M., de Camargo, R., Hodges, K.I., Guedes Soares, C. & da Silva Dias, P.L. (2020b) Atlantic extratropical cyclone tracks in 41 years of ERA5 and CFSR/CFSv2 databases. *Mendely Data*, 4, 108111.
- Gramcianinov, C.B., de Camargo, R., Campos, R.M., Guedes Soares, C. & da Silva Dias, P.L. (2023) Impact of extratropical cyclone intensity and speed on the extreme wave trends in the Atlantic Ocean. *Climate Dynamics*, 60, 1447–1466.
- Grise, K.M., Son, S.-W. & Gyakum, J.R. (2013) Intraseasonal and interannual variability in North American storm tracks and its relationship to equatorial Pacific variability. *Monthly Weather Review*, 141, 3610–3625.
- Guimarães, P., Farina, L. & Toldo, E., Jr. (2014) Analysis of extreme wave events on the southern coast of Brazil. *Natural Hazards and Earth System Sciences*, 14, 3195–3205.
- Hart, R.E. (2003) A cyclone phase space derived from thermal wind and thermal asymmetry. *Monthly Weather Review*, 131, 585–616.
- Heinemann, G. (1990) Mesoscale vortices in the Weddell Sea region (Antarctica). *Monthly Weather Review*, 118, 779–793.
- Hodges, K. (1995) Feature tracking on the unit sphere. *Monthly Weather Review*, 123, 3458–3465.
- Hodges, K. (1996) Spherical nonparametric estimators applied to the UGAMP model integration for AMIP. *Monthly Weather Review*, 124, 2914–2932.
- Hodges, K.I. (1994) A general method for tracking analysis and its application to meteorological data. *Monthly Weather Review*, 122, 2573–2586.
- Hodges, K.I., Lee, R.W. & Bengtsson, L. (2011) A comparison of extratropical cyclones in recent reanalyses ERA-Interim, NASA MERRA, NCEP CFSR, and JRA-25. *Journal of Climate*, 24, 4888–4906.
- Hoskins, B.J. & Hodges, K.I. (2002) New perspectives on the Northern Hemisphere winter storm tracks. *Journal of the Atmospheric Sciences*, 59, 1041–1061.
- Hoskins, B.J. & Hodges, K.I. (2005) A new perspective on Southern Hemisphere storm tracks. *Journal of Climate*, 18, 4108–4129.
- Inatsu, M. & Hoskins, B.J. (2004) The zonal asymmetry of the Southern Hemisphere winter storm track. *Journal of Climate*, 17, 4882–4892.
- Jena, B., Bajish, C., Turner, J., Ravichandran, M., Anilkumar, N. & Kshitija, S. (2022) Record low sea ice extent in the weddell sea, Antarctica in April/May 2019 driven by intense and explosive polar cyclones. *njp Climate and Atmospheric Science*, 5, 19.
- Leal, K.B., Robaina, L.E.d.S., Körting, T.S., Nicolodi, J.L., da Costa, J.D. & Souza, V.G. (2023) Identification of coastal natural disasters using official databases to provide support for the coastal management: the case of santa catarina, Brazil. *Natural Hazards*, 1–18. <https://link.springer.com/article/10.1007/s11069-023-06150-3>
- Mailier, P., Mailier, P.J., Stephenson, D.B., Stephenson, D.B., Ferro, C.A.T., Ferro, C.A.T. et al. (2006) Serial clustering of extratropical cyclones. *Monthly Weather Review*, 134, 2224–2240.
- Mendes, D., Souza, E.P., Marengo, J.A. & Mendes, M.C. (2010) Climatology of extratropical cyclones over the South American-southern oceans sector. *Theoretical and Applied Climatology*, 100, 239–250.
- Michaelis, A.C., Willison, J., Lackmann, G.M. & Robinson, W.A. (2017) Changes in winter North Atlantic extratropical cyclones in high-resolution regional pseudo-global warming simulations. *Journal of Climate*, 30, 6905–6925.
- Murray, R.J. & Simmonds, I. (1991) A numerical scheme for tracking cyclone centres from digital data. Part II: application to January and July general circulation model simulations. *Australian Meteorological Magazine*, 39, 167–180.
- Neiman, P.J. & Shapiro, M. (1993) The life cycle of an extratropical marine cyclone. Part I: frontal-cyclone evolution and thermodynamic air-sea interaction. *Monthly Weather Review*, 121, 2153–2176.
- Parise, C.K., Calliari, L.J. & Krusche, N. (2009) Extreme storm surges in the south of Brazil: atmospheric conditions and shore erosion. *Brazilian Journal of Oceanography*, 57, 175–188.
- Pezza, A.B. & Simmonds, I. (2005) The first South Atlantic hurricane: unprecedented blocking, low shear and climate change. *Geophysical Research Letters*, 32, L15712.
- Pinto, J.G., Spangenberg, T., Ulbrich, U. & Speth, P. (2005) Sensitivities of a cyclone detection and tracking algorithm: individual tracks and climatology. *Meteorologische Zeitschrift*, 14, 823–838.
- Reboita, M., Crespo, N., Dutra, L., Silva, B., Capucin, B. & da Rocha, R. (2021) Iba: the first pure tropical cyclogenesis over the western South Atlantic Ocean. *Journal of Geophysical Research: Atmospheres*, 126, e2020JD033431.
- Reboita, M.S., Da Rocha, R.P., Ambrizzi, T. & Sugahara, S. (2010a) South atlantic ocean cyclogenesis climatology simulated by regional climate model (RegCM3). *Climate Dynamics*, 35, 1331–1347.
- Reboita, M.S., da Rocha, R.P., de Souza, M.R. & Llopis, M. (2018) Extratropical cyclones over the southwestern South Atlantic Ocean: HadGEM2-ES and RegCM4 projections. *International Journal of Climatology*, 38, 2866–2879.
- Reboita, M.S., Gan, M.A., Da Rocha, R. & Ambrizzi, T. (2010b) Precipitation regimes in south america: a bibliography review. *Revista Brasileira de Meteorologia*, 25, 185–204.
- Reboita, M.S., Gozzo, L.F., Crespo, N.M., Custodio, M.d.S., Lucyrio, V., de Jesus, E.M. et al. (2022) From a Shapiro-Keyser extratropical cyclone to the subtropical cyclone raoni: an unusual winter synoptic situation over the South Atlantic ocean. *Quarterly Journal of the Royal Meteorological Society*, 148, 2991–3009.
- Rivals, H., Rivals, H., Cammas, J., Cammas, J.-P., Renfrew, I.A. & Renfrew, I.A. (1998) Secondary cyclogenesis: the initiation phase of a frontal wave observed over the eastern Atlantic. *Quarterly Journal of the Royal Meteorological Society*, 124, 243–267.
- Rudeva, I. & Gulev, S.K. (2007) Climatology of cyclone size characteristics and their changes during the cyclone life cycle. *Monthly Weather Review*, 135, 2568–2587.
- Sanders, F. & Gyakum, J.R. (1980) Synoptic-dynamic climatology of the “bomb”. *Monthly Weather Review*, 108, 1589–1606.
- Savitzky, A. & Golay, M.J. (1964) Smoothing and differentiation of data by simplified least squares procedures. *Analytical Chemistry*, 36, 1627–1639.
- Schemm, S., Sprenger, M. & Wernli, H. (2018) When during their life cycle are extratropical cyclones attended by fronts? *Bulletin of the American Meteorological Society*, 99, 149–165.

- Shapiro, M.A., Doyle, J., Zou, X., Jorgensen, D.P., Jorgensen, D.P. & Jorgensen, D.P. (1997) Extratropical secondary cyclones: simulations and observations.
- Shapiro, M.A. & Keyser, D. (1990) *Fronts, jet streams and the tropopause*. Boston, MA: Springer.
- Simmonds, I. & Keay, K. (2000) Mean Southern Hemisphere extratropical cyclone behavior in the 40-year NCEP–NCAR reanalysis. *Journal of Climate*, 13, 873–885.
- Simmonds, I. & Wu, X. (1993) Cyclone behaviour response to changes in winter Southern Hemisphere sea-ice concentration. *Quarterly Journal of the Royal Meteorological Society*, 119, 1121–1148.
- Sinclair, M.R. (1995) A climatology of cyclogenesis for the Southern Hemisphere. *Monthly Weather Review*, 123, 1601–1619.
- Steele, C., Dorling, S., von Glasow, R. & Bacon, J. (2015) Modelling sea-breeze climatologies and interactions on coasts in the southern North Sea: implications for offshore wind energy. *Quarterly Journal of the Royal Meteorological Society*, 141, 1821–1835.
- Swart, N.C., Fyfe, J.C., Gillett, N. & Marshall, G.J. (2015) Comparing trends in the southern annular mode and surface westerly jet. *Journal of Climate*, 28, 8840–8859.
- Trigo, I.F. (2006) Climatology and interannual variability of storm-tracks in the EURO-Atlantic sector: a comparison between ERA-40 and NCEP/NCAR reanalyses. *Climate Dynamics*, 26, 127–143.
- Turner, J. & Thomas, J.P. (1994) Summer-season mesoscale cyclones in the Bellingshausen-Weddell region of the antarctic and links with the synoptic-scale environment. *International Journal of Climatology*, 14, 871–894.
- Veiga, J.A.P., Pezza, A.B., Simmonds, I. & Silva Dias, P.L. (2008) An analysis of the environmental energetics associated with the transition of the first South Atlantic hurricane. *Geophysical Research Letters*, 35, L15806.
- Vera, C.S., Vigliarolo, P.K. & Berbery, E.H. (2002) Cold season synoptic-scale waves over subtropical South America. *Monthly Weather Review*, 130, 684–699.
- Vihma, T. (2014) Effects of Arctic Sea ice decline on weather and climate: a review. *Surveys in Geophysics*, 35, 1175–1214.

## SUPPORTING INFORMATION

Additional supporting information can be found online in the Supporting Information section at the end of this article.

**How to cite this article:** Couto de Souza, D., da Silva Dias, P. L., Gramcianinov, C. B., da Silva, M. B. L., & de Camargo, R. (2024). New perspectives on South Atlantic storm track through an automatic method for detecting extratropical cyclones' lifecycle. *International Journal of Climatology*, 1–21. <https://doi.org/10.1002/joc.8539>